A Comparison of Methods to Determine Mass Transports from Hydrographic Measurements

J. C. DE MUNCK*

Department of Physical Oceanography, The Netherlands Institute for Sea Research, Den Burg, the Netherlands

(Manuscript received 13 June 1994, in final form 23 December 1996)

ABSTRACT

The purpose of this paper is to discuss the possibility of determining mass transports in a relatively small ocean region, using a hydrographic dataset and some general physical principles. A new hydrographic dataset of the Iceland Basin is used as an example. The physical principles imply geostrophy for the baroclinic component of the velocity field, whereas the barotropic component is determined in the first instance by assuming a uniform level of no motion.

It is attempted to eliminate the subjectivity inherent in this method by using inverse modeling techniques, which describe the physical principles (conservation of tracers) in a mathematical form. In this paper it is shown that some of this subjectivity is misleading, by presenting in detail which choices are to be made and how they influence the results. These choices include weighting parameters, omission of planned measurements, and smoothing parameters.

From a simulation study on the Levitus dataset it is concluded that the stability of the inverse methods can be improved by choosing an alternative way of sampling.

1. Introduction

In this paper, the problem is addressed to estimate geostrophic transports from hydrographic and tracer distribution measurements. In the area of interest, the Iceland Basin (60°–65°N, 10°–30°E), a hydrographic dataset was collected in spring 1990 and 1991. In Fig. 1 the hydrographic stations of the 1991 dataset are plotted on a topographic map. The stations are arranged in boxes that are either closed or bounded by land. Figure 2 shows the 1990 and 1991 stations that are grouped into sections, through which the transports are to be determined. Stations on sections I, II, III, IV, and V of the 1991 dataset have corresponding stations in the 1990 dataset that are closer than 2 km. One of the aims of the measurement program was to obtain more insight in the size, location, and branching of the overflow transport and the deep northern boundary current (McCartney 1992). In particular, it was hoped to quantify some of the water movements determined by a water mass analysis (van Aken and de Boer 1993, unpublished manuscript, hereafter VADB) of the same dataset.

The main topic of the present paper is concerned with the possibility of answering the above research questions in an objective way, thereby only using the regional dataset and some general physical principles. To obtain an independent view the a priori knowledge from other researchers who collected data in the same area is avoided.

The hydrographic data alone give, through the geostrophic and hydrostatic approximation of the momentum equation, a relationship between the vertical derivative of the horizontal velocity field and the horizontal density gradient: the thermal wind balance. The integration constant, necessary to compute the velocity field itself, may vary with the horizontal position. The classical way to find the integration constant is to assume that at a certain pressure level p_0 the velocity vanishes. The subjectivity in this solution originates from the assumption that there *is* a uniform level of no motion [which is questionable on theoretical grounds, Olbers and Willebrand (1984)], and, if it exists, where it should be chosen. The ambiguity in the latter problem can be removed by choosing the level of no motion such that the net mass flux into a closed box is minimized.

In 1978 Wunsch proposed an inverse modeling technique to remove the subjectivity inherent to the assumption of a level of no motion. In this method, the missing integration constants are found by taking into account that some of the tracers are conservative, so that the net amount of tracer material flowing into a bounded region is zero. By translating these kinds of

* Current affiliation: MEG Center KNAW, Amsterdam, the Netherlands.

Corresponding author address: Dr. Jan C. de Munck, MEG Center KNAW, AZVU Reception C, De Boelelaan 1117, Amsterdam 1081 HV, the Netherlands.
E-mail: 76511.3025@compuserve.com

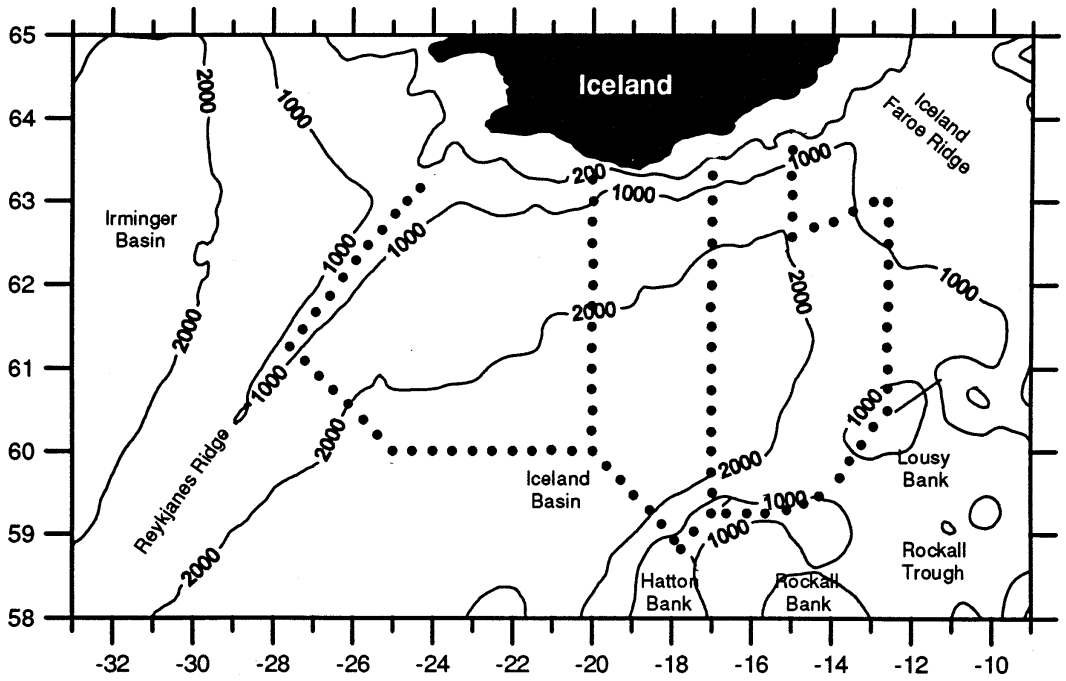

FIG. 1. The bottom topography of the Iceland Basin with the locations of the 1991 stations. Isobaths are presented in meters.

restrictions for different tracers and different regions into a set of mathematical equations in which the integration constants act as the unknowns, the total flow can be computed by solving these equations, at least in principle. In practice, however, the mathematical constraints resulting from the conservation assumptions often appear to be linearly dependent, and therefore there is generally no unique solution.

At first glance, it might seem hopeless to try to solve an underdetermined system of equations. There are,

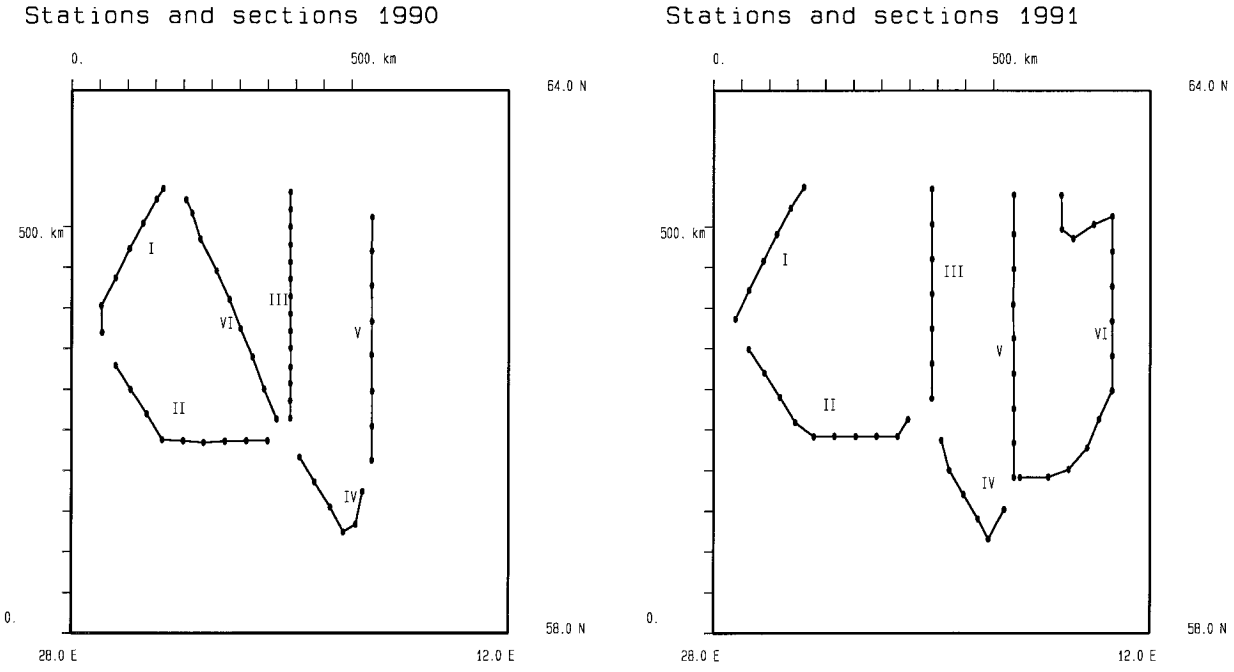

FIG. 2. Schematic locations of the stations and sections of the 1990 (left) and 1991 (right) dataset. The positions of the stations corresponding to one section have been blown up a little. In reality, the last station of section I coincides with the first station of section II.

however, reasons why the situation in the particular case of the hydrographic inverse problem is different. In the first place, one could select the large-scale solution using a singular value decomposition (SVD) of the model equations. Wunsch (1978), Fu (1981), and Roemmich (1980, 1981) argue that the SVD solution chooses, among all possible solutions, the one in which the small-scale variations are filtered out. In the second place, oceanographers are generally only interested in the total transports through sections, rather than in the velocities at individual station pairs. In this way, the number of degrees of freedom is substantially reduced.

Since the SVD method selects, among all possible barotropic flows satisfying the inverse model equations, the one that has minimum norm in a least squares sense, an alternative argument for the SVD solution is that it gives the flow with the least kinetic energy (e.g., Van Aken 1988). An important feature of the SVD solution is that it depends on a reference level used to compute the baroclinic velocity. This reference level can be considered as a source of subjective input from the researcher. For example, the ''large-scale interpretation'' of Wunsch and the ''minimum kinetic energy interpretation'' only work at this reference level. Another point of concern is that for a large-scale filter, one would prefer to minimize the horizontal derivative in flow, instead of its amplitude. This idea has been put forward before (e.g., Wunsch 1978; Stommel and Veronis 1981) and in McIntosch (1990) a formal relationship between type of norm and length scale is given, but, as far as the author knows, it has not yet been worked out in detail for the problem at hand.

The interpretation of Fiadeiro and Veronis (1982) of the SVD solution is that it determines the smallest possible correction to the classical level of no motion approach that is necessary to satisfy conservation principles. The dependence of the SVD solution on the initial reference pressure is used to minimize the correction. Another variant is sketched in Veronis (1987). First, a level of no motion is sought, which conserves mass as well as possible. Then, using this level as a reference for the baroclinic velocity, the smallest possible correction to this initial choice is computed by using the SVD method. Both variants seem to solve the reference problem but it still remains unclear what the underlying physical principles are that lead to the proposed two-step method. The implicit assumption that there *is* a uniform level of ''slow motion,'' which conserves mass (although it is at unknown depth) enormously restricts the solution space and overdetermines the system of equations. But at the same time the physical basis underlying this assumption may be called questionable. In the present paper an alternative method is shown that avoids the arbitrariness of the reference level.

In the next section, the solution determined by an optimal level of no motion will be presented and discussed. Then it will be attempted to improve this solution using inverse modeling techniques. In section 3, these techniques are analyzed in detail and its underlying assumptions are made explicit. In section 4, the results of several variants of inverse models are presented, compared, and discussed. In section 5, a simulation study is presented on an alternative way of sampling, which yields more stable equations in which the unwanted sensitivities are substantially reduced.

2. The optimal level of no motion

The sampling scheme of hydrographic data intended for inverse modeling usually consists of a set of vertical sections that enclose one or more water volumes (boxes). At the vertical boundaries of these boxes the in situ density ρ can be determined from temperature and salinity measurements as a function of pressure p. Since the density is measured as a function of pressure, and not as function of geopotentials, the geostrophic flow through the boundary can only be computed with an arbitrary offset. This offset appears in the geostrophic–hydrostatic equations if they are transformed into a coordinate system in which the pressure (instead of the geopotential) acts as a vertical coordinate. If s is the horizontal coordinate along a section, then the geostrophic flow perpendicular to the curve γ: $x = x(s)$, $y = y(s)$ is given by

$$v(s, p) = \frac{1}{f}\frac{\partial}{\partial s}\left\{\int_{p_0}^{p} \frac{dp'}{\rho(s, p')} - g\zeta_0(s)\right\}. \qquad (1)$$

Here $\zeta_0(s)$ is the unknown height of a (yet) arbitrary pressure level p_0 over an equipotential surface of the earth's gravity field, f is the Coriolis parameter, and g is the gravity acceleration. The positive flow direction of v with respect to the curve is to the right-hand side for increasing s.

If there is a uniform level of no motion at $p = p_0$, then $\zeta_0(s) = 0$ for all s. Geostrophic velocities at a pressure level p can be computed by integrating the gradient of the specific volume anomaly from p_0 to p. With these velocities, the corresponding net mass transport of a box of Fig. 2 will, in general, not vanish, which violates the conservation of mass applied to that box. The optimal level is determined by varying p_0 in such a way that the sum of squared net transports (the rms value) is minimum.

a. Results

Using the bisection method, it was found that for the 1990 dataset the optimal level of no motion is at 958 dbar and the rms value of the net transports is 0.69 (Sv $\equiv 10^6$ m^3 s^{-1}). For the 1991 dataset these numbers are 1009 dbar and 1.20 Sv. These results imply that at some stations the level of no motion was deeper than the station depth. At these stations p_0 was set to station depth. In Fig. 3 the transports through each of the sec-

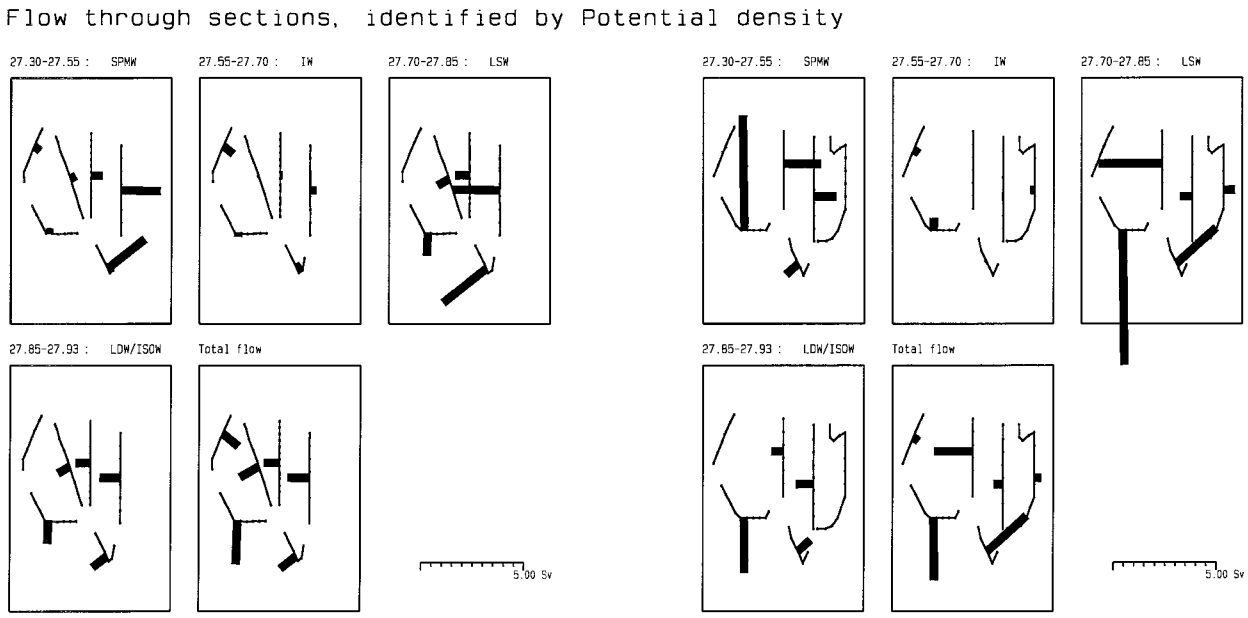

FIG. 3. Transports in 1990, computed by a uniform optimal level of no motion at 958 dbar (left) and with a level of no motion at 1009 dbar for the 1991 data (right).

tions are graphically presented (left 1990, right 1991). For this purpose, the water column is divided into four layers, bounded by a surface of constant potential density (relative to the 0 dbar level): first layer, 27.30–27.55; second layer, 27.55–27.70; third layer, 27.70–27.85; and the fourth layer, 27.85–27.93 (bottom). In Fig. 4 the isopycnals are given for each box boundary. The first layer roughly corresponds to sub-polar mode water (SPMW), the second layer corresponds to intermediate water (IW), the third layer corresponds to Labrador Sea Water (LSW), and the fourth layer corresponds to the lower deep water (LDW) and the Iceland–Scotland overflow water (ISOW) (VADB). For each layer, the transports through each section are presented within a box in Fig. 3. The length of the black bars gives the volume of the transport; the scale is given in the lower right corner of the figure. The lower middle box gives the total transports through each of the sections. Table 1 gives the total transports for 1990, compared to those for 1991.

b. Discussion

From these results three conclusions may be drawn:

1) With the simple concept of a level of no motion very small mass deficits can be obtained.
2) The transports of corresponding sections all have the same sign (except section IV) and the same order of magnitude.
3) The location of the optimal level of no motion is rather constant.

Furthermore, in both datasets the upper layer, representing the SPMW, is flowing toward the northeast and at the bottom a return current is flowing toward the south. This roughly confirms the qualitative ideas about the area as presented in, for example, Harvey and Theodoroy (1986).

The results presented in Fig. 3 also demonstrate that the mass deficit for the individual layers is quite large. For instance, in the upper layer of the leftmost box of the 1991 dataset, the transport over the Reykjanus Ridge (section I) is virtually zero whereas the difference in transport through this layer of the remaining two sections amounts to 2.3 Sv. The mass deficit in the lower two layers is of the same order but of opposite sign. Therefore, the total mass deficit of box I is only 0.06 Sv. Similar effects play a role in the other two boxes. These results can only be explained by a vertical advection across an isopycnal surface of about 2 Sv in the left box. Vertical transports of this size roughly correspond to an average vertical velocity of 5.0×10^{-5} m s^{-1}, if an area of 200×200 km^2 is assumed. This number is quite large because it is comparable to the total vertical motion, which typically amounts to 10^{-6} to 10^{-4} m s^{-1} (e.g., Apel 1987).

A more fundamental objection against these results is that they are based on the existence of a uniform level of no motion. Although the current meter measurements carried out in the Iceland Basin (Van Aken 1997, manuscript submitted to *J. Phys. Oceanogr.*) seem to indicate that there is a minimum velocity at 1000 dbar, when the amplitudes of all moorings are plotted in one figure against pressure, this does not necessarily imply that the there is a *uniform* level of no motion. An alternative method to investigate the water movement as a function

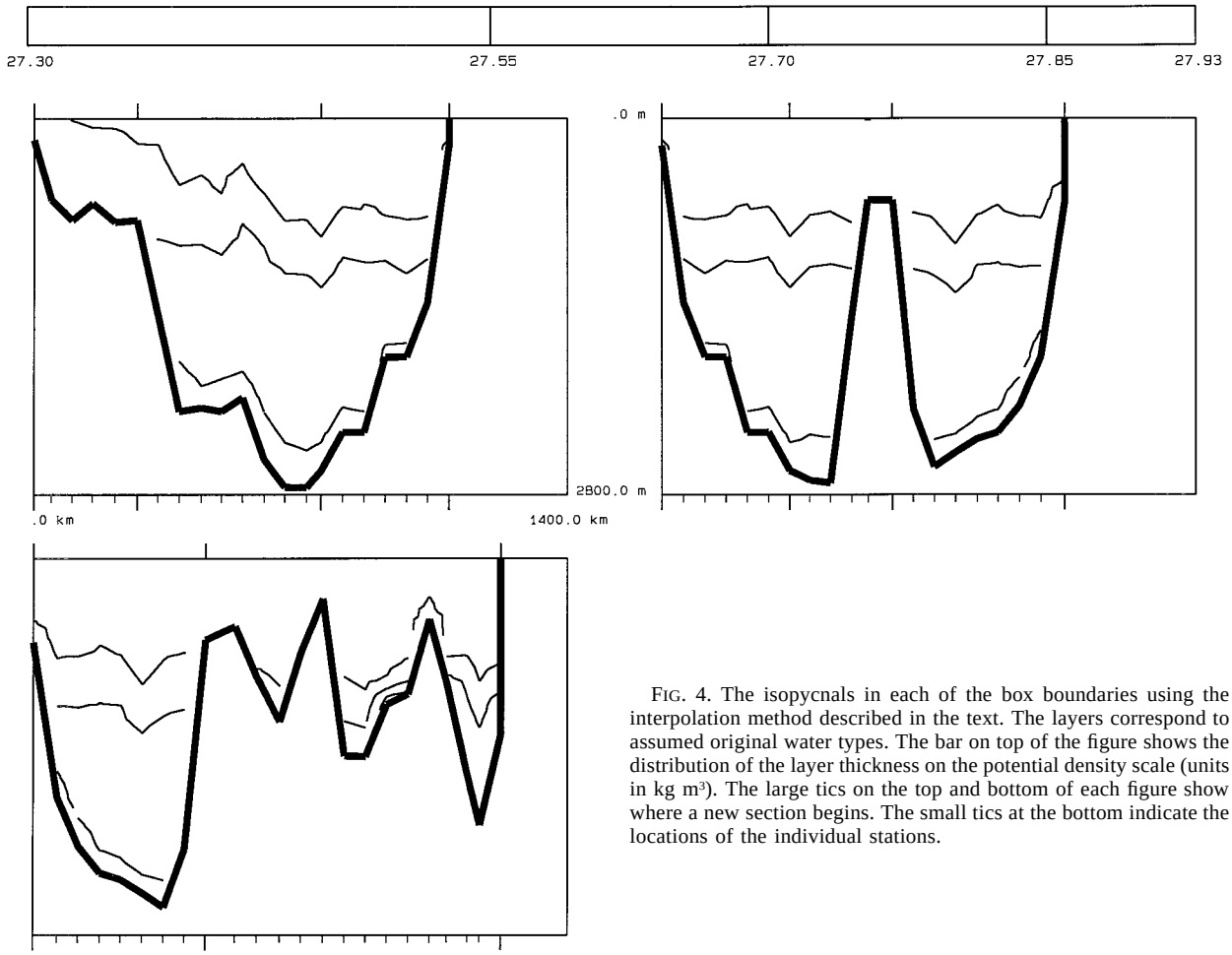

FIG. 4. The isopycnals in each of the box boundaries using the interpolation method described in the text. The layers correspond to assumed original water types. The bar on top of the figure shows the distribution of the layer thickness on the potential density scale (units in kg m^3). The large tics on the top and bottom of each figure show where a new section begins. The small tics at the bottom indicate the locations of the individual stations.

of depth, with the given two datasets, is to plot the temporal variability of the tracer measurements as a function of depth. If it is assumed that temporal variability of the tracers is mainly determined by advection of horizontal gradients and if, moreover, the horizontal gradients are roughly depth independent, then one would expect to find a *minimum* in variability at $p =$ 1000 dbar.

Figure 5 shows the difference in salinity, oxygen, silicate, nitrate, potential temperature and potential density between the 1990 and the 1991 dataset as a function of depth. All stations selected are deeper than 1500 dbar, and have a counterpart of the complementary dataset closer than 4 km. There were 22 station pairs meeting these requirements. The level of *maximum* variability in all tracers presented is approximately 800 dbar, which is rather close to the optimal level of no motion. Figure 5 shows that the level of minimum variability, if it exists, is below 1500 dbar.

When all six tracers in all 22 station pairs are considered as independent samples, it is rather contradictory to find a maximum variability close to 1000 dB if at the same time it is assumed that the water is motionless at that level. This analysis demonstrates the need for an inverse method, in which the level of no motion is avoided.

3. The inverse method

a. Assumptions

The purpose of inverse methods, applied to the problem of transport estimation, is to improve the method of a uniform level of no motion. In the inverse method, as introduced and developed by Wunsch (1978), the barotropic component is estimated from a mathematical model describing the measured tracer concentrations C. This model is based on the assumptions that the tracer is conservative. In integral form, this assumption can be stated as

$$\int\int_S (C\mathbf{v} - \vec{\kappa}\,\mathrm{grad}C)\cdot d\vec{\sigma} + \int\int\int_{\mathrm{box}} \frac{\partial C}{\partial t}\, d^3x = 0. \quad (2)$$

Here, S is total boundary of the box.

TABLE 1. Total transports in 1990 and 1991 through each section (Sv) and the net transports (Sv) into each of the three boxes.

	Transports through section					Net transports		
	I	II	III	IV	V	Left	Middle	Right
1990	.89	−1.55	−.77	−.88	−1.09	.33	−.22	−.56
1991	.28	−2.23	−1.89	2.30	−.47	−.06	.88	.81
	E	N	E	N	E	in	in	in

In Wunsch (1978) and others, this equation is applied in the following form:

$$\iint_{S_{\text{vert}}} C\mathbf{v}\cdot d\vec{\sigma} = 0, \tag{3}$$

where S_{vert} is the vertical boundary of the box or the vertical boundary of a box bounded by two levels of constant tracer concentration.

In the following it will be shown which assumptions are underlying the approximation of (2) in the form of (3). First, it will be assumed that the box extends from top to bottom and then it will be shown which additional assumptions are to be made to divide the box into layers. Equation (2) can be split into the following five terms:

$$\iint_{S_{\text{vert}}} C\mathbf{v}\cdot d\vec{\sigma} - \iint_{S_{\text{vert}}} (\vec{\vec{\kappa}}\,\text{grad}C)\cdot d\vec{\sigma} + \iint_{S_{\text{hor}}} C\mathbf{v}\cdot d\vec{\sigma} - \iint_{S_{\text{hor}}} (\vec{\vec{\kappa}}\,\text{grad}C)\cdot d\vec{\sigma} + \iiint_{\text{box}} \frac{\partial C}{\partial t}\, d^3x = 0. \tag{4}$$

The first term of Eq. (4) is built up from, say, three or four vertical boundaries with a typical size of $H_B L_B CV$ each, where H_B and L_B are the height and length scale of the box, C is the typical tracer concentration, and V is the typical velocity scale. In order to neglect the other four terms with respect to the first it has to be demonstrated that each of these integrals is much smaller than $H_B L_B CV$.

For the size of the second term, one finds $H_B L_B \kappa_L \Delta C_L / L_C$. Here $\Delta C_L/L_C$ is the typical horizontal tracer gradient. The vertical diffusion does not contribute because the vertical tracer gradient is parallel to the vertical surface. Therefore, the horizontal diffusion can be neglected with respect to horizontal advection, provided that

$$\kappa_L \ll L_C VC/\Delta C_L. \tag{5}$$

Using $L_C = 50$ km, $\Delta C/C = 0.1$, and $V = 0.2$ m s^{-1}, this condition is satisfied for $\kappa_L \ll 10^5$ m^2 s^{-1}. If C represents the density, $\Delta C/C = 10^{-4}$ might be more realistic, and it is even found that $\kappa_L \ll 10^8$ m^2 s^{-1}. The standard value for κ_L given in LeBlond and Mysac (1978) ranges from 10^2 to 10^6 m^2 s^{-1}. With the density as tracer, the required upper limit of κ_L is almost certainly larger than the true value, so that horizontal diffusion can be neglected without much concern.

When the box stretches from top to bottom, the third and fourth integrals vanish, because $w = 0$ and $\partial C/\partial z = 0$ at the top boundary and at the bottom we have $w + (u, v)\nabla_2 H = 0$ and $\partial C/\partial \mathbf{n} = 0$. The size of the fifth term can be estimated as $H_B L_B^2 \Delta C_T/T$, where ΔC_T is a typical scale for concentration changes on a timescale T. Therefore, the time-dependent term may be left out of the balance, when

$$T \gg L_B \Delta C_T/CV. \tag{6}$$

For $L_B = 500$ km and $V = 0.2$ m s^{-1}, $\Delta C/C = 0.1$ the tracer should be stationary for timescales of at least 3 days. For smaller boxes, this requirement becomes proportionally less restrictive.

When S_{vert} stretches from top to bottom, we have only one restrictive equation for the velocity field, for each conservative tracer and for each box. If, however, in addition to the aforementioned assumptions the tracer under consideration has a vertical advection and diffusion that is small with respect to the horizontal advection balance, the surface S_{vert} can be subdivided into smaller parts, yielding more equations per box. We now have to consider under which conditions the third and fourth terms of (4) are small compared to the first, when the horizontal boundary is defined by a surface on which C is constant.

The amplitude of the vertical motion could be estimated by the β effect as has been done by Tziperman and Hecht (1988) but in the area examined here this estimate would be much too small. The Iceland Basin is characterized by the presence of overflow water, flowing over the bottom topography thereby conserving its potential density. Due to the large bottom topography the vertical motion is much larger than the β-effect estimate. If the ''quasi-horizontal'' boundaries of the boxes are defined by S_{hor}: $C(\mathbf{x}, t_0) = C$, with t_0 the time instant at which the measurements are done, then the motion perpendicular to this surface can be expressed in the time derivatives of the tracers. The normal of the quasi-horizontal surface is directed parallel to the gradient of the concentration and therefore its surface elements $d\vec{\sigma}$ are given by $(\text{grad}C/|\text{grad}C|)\, d\sigma$. The vertical advection through a surface of constant concentration is given by

$$\iint_{S_{\text{hor}}} C\mathbf{v}\cdot d\vec{\sigma} = \iint_{S_{\text{hor}}} \frac{C}{|\text{grad}C|}\left(\frac{dC}{dt} - \frac{\partial C}{\partial t}\right) d\sigma. \tag{7}$$

This equation, which is exact, expresses the vertical transport in terms of tracer gradients and time derivatives. Therefore, we found for the size of the vertical transport $CL_B^2(\text{H}_C/\Delta C_H)(\Delta C_T/T)$, where T is the timescale

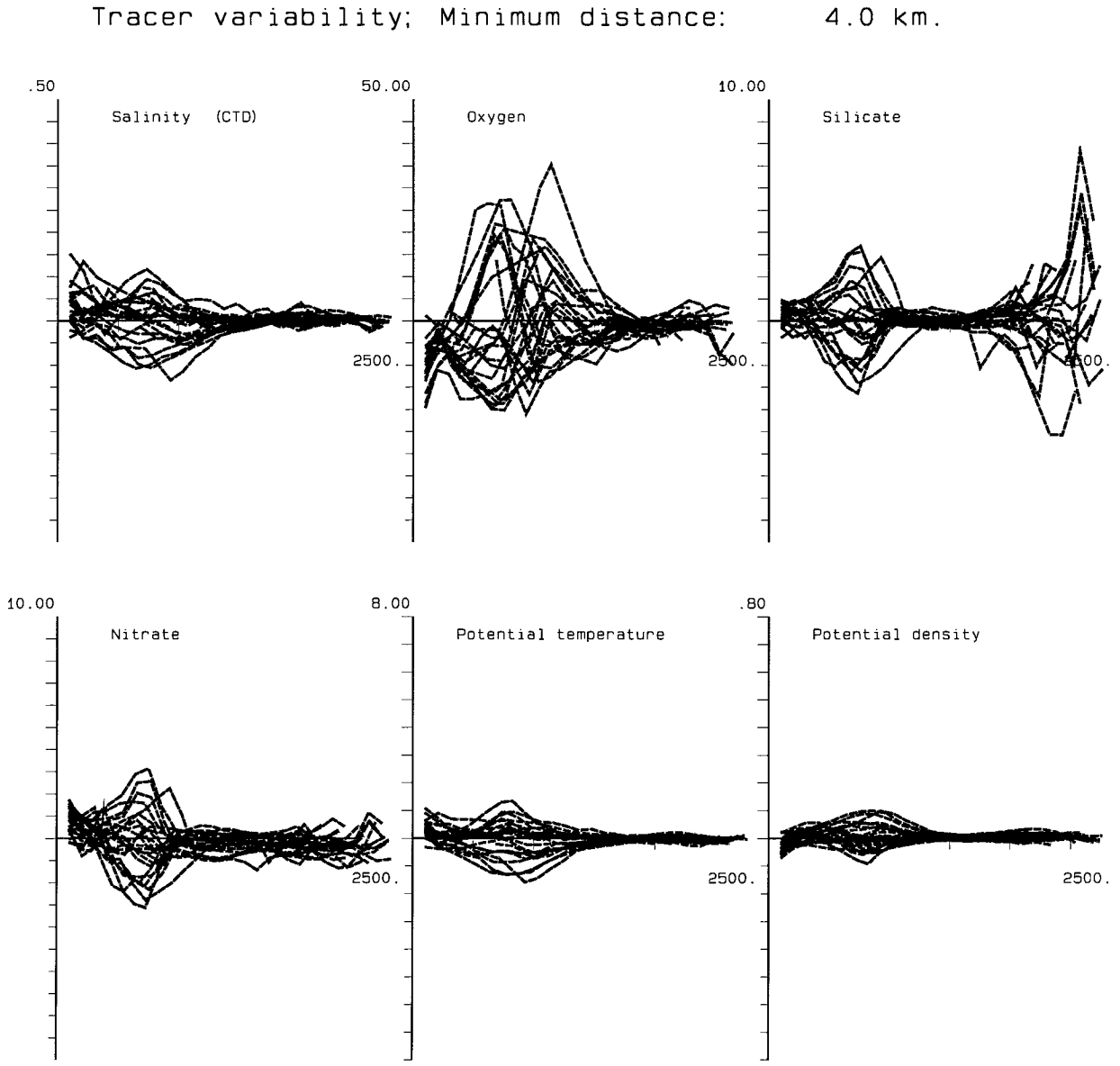

FIG. 5. Temporal variability as a function of pressure. See text.

of tracer variation. The vertical advection is small compared to the horizontal advection ($\sim CVH_B L_B$ with H_B the thickness of the layer) if the timescale

$$T \gg L_B H_C \Delta C_T / H_B V \Delta C_H. \tag{8}$$

With $L_B = 500$ km, $H_C = 200$ m, $H_B = 200$ m, $V = 0.2$ m s^{-1}, and $\Delta C_T = \Delta C_H$, we find $T \gg 30$ days. So if C represents the potential density, and if C varies 0.2 kg m^{-3} over a vertical distance of 200 m (see Fig. 4), then the temporal variation in C should be much smaller than 0.2 kg m^{-3} in 30 days. Figure 5 shows that in the deeper waters the differences in potential density over a year are generally smaller than 0.2 kg m^{-3}. However, if these changes are due to seasonal variations, then the water might reach a density change of 0.2 kg m^{-3} much faster than in 30 days.

The vertical diffusion through the horizontal surface [fourth term in Eq. (4)] is of the order of $L_B^2 \kappa_H \Delta C_H / H_C$. Compared to the horizontal advection balance, this effect is small, provided that

$$\kappa_H \ll H_C V H_B C / \Delta C_H L_B. \tag{9}$$

With $H_C = 200$ m, $V = 0.2$ m s^{-1}, $H_B = 200$ m, $\Delta C/C = 0.1$, and $L_B = 500$ km, we find that $\kappa_H \ll 0.16$ m^2 s^{-1}. When this upper bound is compared with the figures given in LeBlond and Mysak (1978), $\kappa_H = 3 \times 10^{-5}$ to 2×10^{-2} m^2 s^{-1}, it appears that vertical diffusion

plays no important role in the approximation of (2) as a horizontal advection balance.

If the tracer balance is completely determined by the horizontal advection, we find

$$\iint_{S_{\text{vert}}^{(n)}} C\mathbf{v} \cdot d\vec{\sigma} \approx C \iint_{S_{\text{vert}}^{(n)}} \mathbf{v} \cdot d\vec{\sigma} = 0. \qquad (10)$$

The final approximation made here has a purely mathematical background. The tracer concentration C always varies between two almost equal positive constants, whereas $\mathbf{v} \cdot d\vec{\sigma}$ may have changes in sign. Therefore, the tracer concentration may be placed in front of the integral sign. If C refers to potential temperature, and if the upper side and the lower side of the layer are determined by 10°C and 8°C, then inside the layer C can be considered as constant. For density and salinity tracers this approximation holds even better. Note that, although the symbol C does not appear in the final approximation (10), the balance still depends on the tracer concentration because its value determines the precise shape of the upper and lower boundary of the layer.

Equation (10) yields one restriction for each tracer, for each box and for each layer (referred to by n) into which the box is subdivided. The most critical assumption appeared to be the stationarity of the tracers, when a subdivision into layers is made. When the box extends from top to bottom, the horizontal diffusion might be problematic for some tracers, but not for density. The stationarity of the complete box requires a timescale of three days, which is much smaller than the timescale required to treat the whole dataset as synoptic.

To obtain equations restricting the barotropic current pattern, (10) is used with the geostrophic flow substituted for **v**, split into an unknown barotropic part and a known baroclinic part. If the tracer happens to be solely dependent on pressure and if the box has no bottom topography, then (10) is automatically satisfied because of the geostrophic degeneration. Therefore, inverse equations in the form of (10) can only restrict the barotropic current pattern if there is a large bottom topography or a horizontally inhomogeneous tracer.

b. Implementation

The theoretical model equations given in section 2 are valid for continuous fields and take on the form of differentials and integrals. The data, on the other hand, consist of tracers measured at discrete points in 3D space. To apply the theory to a given dataset, the data should be interpolated by which it is transformed into continuous fields. Another reason to consider the interpolation carefully is that the inverse equations are automatically satisfied when the layers have uniform thicknesses and the boxes are not bounded by land. Only deviations from this geometry yield nontrivial restrictions for the barotropic component.

In this paper, the interpolation is based on a triangulation of the data points. This implies that the data points are connected by hypothetical triangles (see Fig. 6) on which the tracer function is interpolated linearly, in a very similar way as with finite element methods. The details of the method are mentioned in the appendix.

When the component of the geostrophic velocity normal to the box boundary is denoted by $v(s, p)$ and when the baroclinic and barotropic parts are denoted by $\tilde{v}(s, p)$ and $\hat{v}(s)$ respectively, then the modeling equation derived in section 3a can be stated as follows:

$$\iint_{S_{\text{vert}}^{(n)}} v \, d\sigma = \iint_{S_{\text{vert}}^{(n)}} (\tilde{v} + \hat{v}) \, d\sigma = 0, \qquad (11)$$

where $S_{\text{vert}}^{(1)}$, $S_{\text{vert}}^{(2)}$, $S_{\text{vert}}^{(3)}$, etc. are the vertical parts of the layers in the different boxes. In order to discretize this equation it is assumed that $\hat{v}$ is constant between two subsequent stations and its value is denoted by $\hat{v}_m$. This assumption is equivalent to the assumption that the dynamic topography $\zeta_0(S)$ is a piecewise linear function. Finally when $S_{\text{vert}}^{(n)}$ is partitioned into $S_1^{(n)}$, $S_2^{(n)}$, . . . , $S_M^{(n)}$, corresponding to the station pairs m, we can write

$$\sum_{m=1}^{M} a_{nm} \hat{v}_m = b_n, \qquad (12)$$

with

$$a_{nm} = \iint_{S_m^{(n)}} d\sigma, \qquad b_n = -\sum_{m=1}^{M} \iint_{S_m^{(n)}} \tilde{v} \, d\sigma. \qquad (13)$$

The proper sign of a_{nm} and b_n depends on the direction of positive flow compared to the direction of the outward normal of the boundary.

Since many tracers may have very similar distributions, the ''inverse equations'' may be linearly dependent and the inverse relations might be insufficient to determine a unique solution. Moreover, in a realistic measurement situation, it might happen that equations contradict each other so that no solutions exist at all, even if there are more unknowns than equations. The latter problem is solved by adding a noise term that accounts for the model misfit. In matrix form this can be expressed as follows:

$$\mathbf{A}\hat{\mathbf{v}} = \mathbf{b} + \varepsilon. \qquad (14)$$

When $|\varepsilon|^2$ is minimized, it is found that $\hat{\mathbf{v}}$ satisfies

$$\mathbf{A}^{\mathrm{T}}\mathbf{A}\hat{\mathbf{v}} = \mathbf{A}^{\mathrm{T}}\mathbf{b}. \qquad (15)$$

Equation (15) has at least one solution, but generally more than one.

In order to determine the complete class of solutions, it is useful to perform a singular value decomposition on the matrix $\mathbf{A}$ (e.g., see Lee 1993)

$$\mathbf{A} = \mathbf{U}\Lambda\mathbf{V}^{\mathrm{T}}. \qquad (16)$$

The number of equations N (number of rows of $\mathbf{A}$) equals the total number of layers in all boxes. The number of unknowns M (number of columns of $\mathbf{A}$) equals

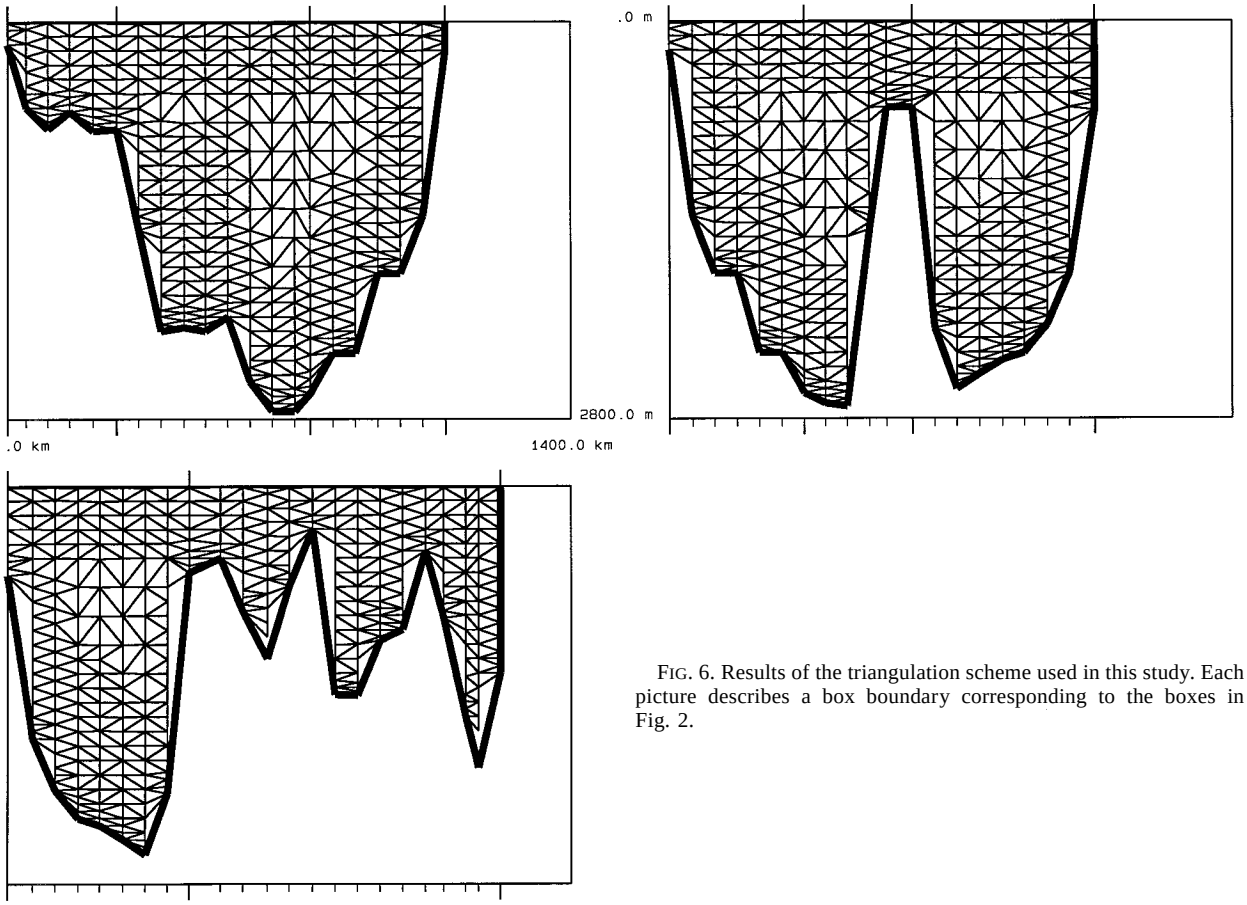

FIG. 6. Results of the triangulation scheme used in this study. Each picture describes a box boundary corresponding to the boxes in Fig. 2.

the number of station pairs. There are different conventions in literature concerning the precise definition of $\mathbf{U}$, $\mathbf{\Lambda}$, and $\mathbf{V}$. In this paper the matrix $\mathbf{V}$ is square and orthonormal: $\mathbf{V}^T\mathbf{V} = \mathbf{V}\mathbf{V}^T = \mathbf{I}_M$ and $\mathbf{\Lambda}$ is a square diagonal matrix with non-negative numbers on the diagonal, ordered in decreasing order. Here it will be assumed that there are more unknowns than equations, so that $M \geq N$. This implies that $\mathbf{U}$ is column orthonormal, or $\mathbf{U}^T\mathbf{U} = \mathbf{I}$ and that there are at least M–N zeros on the diagonal of $\mathbf{\Lambda}$. In the subsequent analysis it will be more convenient to deal with a row-orthonormal matrix $\mathbf{U}$, and therefore as many zero rows are added to $\mathbf{A}$ (and zero entries to $\mathbf{b}$) until $N = M$. In this particular case $\mathbf{U}$ is square and it is both row- and column- orthogonal, so that $\mathbf{U}\mathbf{U}^T = \mathbf{U}^T\mathbf{U} = \mathbf{I}$. Note that the meaning of the symbols $\mathbf{U}$, $\mathbf{\Lambda}$, and $\mathbf{V}$ is different from that in, for example, Wunsch (1978).

The physical dimension of the singular values is meters squared. But since $\Sigma\, \lambda_k^2 = \mathrm{Tr}\{\mathbf{A}^T\mathbf{A}\}$, which follows directly from (16), it is more convenient to express the squares of the singular values as a percentage of the ''total power'' of $\mathbf{A}$, that is, as a percentage of $\mathrm{Tr}\{\mathbf{A}^T\mathbf{A}\}$.

Since $\mathbf{V}$ contains as many columns as there are singular values, we can associate each column of $\mathbf{V}$ with a singular value. When the columns of $\mathbf{V}$ corresponding to a zero singular value are put together in a matrix $\mathbf{V}_0$, the columns of $\mathbf{V}_0$ span the null space of $\mathbf{A}$ and we have $\mathbf{A}\mathbf{V}_0 = 0$. Using $\mathbf{V}_0$ and the SVD of $\mathbf{A}$, the general solution of the minimization problem can be represented as

$$\hat{\mathbf{v}} = \mathbf{V}\tilde{\mathbf{\Lambda}}\mathbf{U}^T\mathbf{b} + \mathbf{V}_0\mathbf{l}. \tag{17}$$

Here the first term is a particular solution and the second term is the general solution of the homogeneous problem. Furthermore, $\tilde{\mathbf{\Lambda}}$ is obtained from $\mathbf{\Lambda}$ by replacing the zeros on the diagonal by infinite numbers, so that its inverses vanish. In formulas,

$$\mathbf{\Lambda} = \begin{pmatrix} \lambda_1 & & & \mathbf{0} \\ & \lambda_2 & & \\ & & \lambda_3 & \\ & & & \ddots \\ \mathbf{0} & & & 0 \\ & & & & 0 \end{pmatrix}, \quad \tilde{\mathbf{\Lambda}} = \begin{pmatrix} \lambda_1^{-1} & & & \mathbf{0} \\ & \lambda_2^{-1} & & \\ & & \lambda_3^{-1} & \\ & & & \ddots \\ \mathbf{0} & & & 0 \\ & & & & 0 \end{pmatrix} \tag{18}$$

and

$$\mathbf{\Lambda\tilde{\Lambda}} \equiv \mathbf{J}_K = \begin{pmatrix} 1 & & & & \\ & 1 & & \mathbf{0} & \\ & & 1 & & \\ & & & \ddots & \\ & \mathbf{0} & & & 0 \\ & & & & & 0 \end{pmatrix}. \tag{19}$$

Here, $\mathbf{J}_K$ is a square diagonal matrix with K ones and M–K zeros on the diagonal. The number of nonzero elements of Λ, $\tilde{\mathbf{\Lambda}}$, and $\mathbf{J}_K$ equals the rank K of the matrix $\mathbf{A}$.

c. Modeling the null space

Equation (17) shows that there is an arbitrariness in the barotropic flow if some of the singular values vanish. The more vanishing singular values, the larger the ambiguity. A generally applied way to handle this ambiguity is to express the norm of $\hat{\mathbf{v}}$ in the vector $\mathbf{l}$, and to minimize it:

$$|\hat{\mathbf{v}}|^2 = |\tilde{\mathbf{\Lambda}}\mathbf{U}^{\mathrm{T}}\mathbf{b}|^2 + |\mathbf{l}|^2, \tag{20}$$

and the vector, which minimizes $|\varepsilon|^2$ and which has minimum norm, is found simply by setting $\mathbf{l} = 0$ in (17):

$$\hat{\mathbf{v}}_0 = \mathbf{V}\tilde{\mathbf{\Lambda}}\mathbf{U}^{\mathrm{T}}\mathbf{b}. \tag{21}$$

This solution is the one that minimizes the motion at the pressure level p_0. As discussed in the introduction, there are objections to this kind of solution. First, there is no objective (physical) argument for minimizing the norm of the solution and, second, the solution will depend on the reference pressure p_0, which was arbitrarily chosen. In addition, as argued by Wunsch (1978), the transports computed with the barotropic flow tend to be unrealistically large at deep stations because in the minimization of (20) the shallower stations obtain a barotropic component of the same order as the deeper stations. Therefore, according to Wunsch, not $|\hat{\mathbf{v}}|^2$ should be minimized, but $|\mathbf{W}\hat{\mathbf{v}}|^2$, where $\mathbf{W}$ is a well-chosen weighting matrix that emphasizes the deeper stations. The mathematical problem of minimizing the weighted norm over all vectors minimizing the error $\boldsymbol{\varepsilon}^{\mathrm{T}}\boldsymbol{\varepsilon}$ can be solved by transforming $\mathbf{A}$ into $\mathbf{A}' = \mathbf{A}\mathbf{W}^{-1}$ and $\mathbf{b}$ into $\mathbf{b}' = \mathbf{W}\mathbf{b}$ and then using the normal procedure to find the minimum norm solution of the primed system. This only works if the inverse of $\mathbf{W}$ exists.

Here, a more general criterion is proposed. With this criterion it is attempted to 1) circumvent the choice of the a priori pressure level p_0 and 2) to minimize the jumps in the total geostrophic flow caused by the linear interpolation technique. The latter aim can be considered as a *maximum smoothness criterion.* To meet these goals the solution of the following problem is studied:

$$\mathbf{H}(\hat{\mathbf{v}}) = \min|\mathbf{D}\,\hat{\mathbf{v}} - \mathbf{c}|^2$$
$$\mathbf{A}^{\mathrm{T}}\mathbf{A}\hat{\mathbf{v}} = \mathbf{A}^{\mathrm{T}}\mathbf{b}, \tag{22}$$

where $\mathbf{D}$ and $\mathbf{c}$ will be chosen such that the resulting velocity field has maximum smoothness. The choice of Wunsch results by taking $\mathbf{D} = \mathbf{W}$ and $\mathbf{c} = \mathbf{0}$. Note that $\mathbf{H}(\hat{\mathbf{v}})$ is minimized over all vectors that minimize the error in the inverse equations. Here it is not required that the inverse of $\mathbf{D}$ exists, and therefore (25) can be considered as a seminorm (e.g., Berthero et al. 1988). The only requirement is that the null space of $\mathbf{W}$ and the null space of $\mathbf{A}$ do not coincide (McIntosh 1990).

The problem posed in (22) is most easily solved by using the general solution (17). After substituting (17) into (22), the value of $\mathbf{l}$ can be determined for which $\mathbf{H}$ is minimum. This minimum can be found by differentiation. The result is

$$\hat{\mathbf{v}} = \hat{\mathbf{v}}_0 - \mathbf{V}_0(\mathbf{V}_0^{\mathrm{T}}\mathbf{D}^{\mathrm{T}}\mathbf{D}\mathbf{V}_0)^{-1}\mathbf{V}_0^{\mathrm{T}}\mathbf{D}^{\mathrm{T}}(\mathbf{D}\hat{\mathbf{v}}_0 - \mathbf{c}). \tag{23}$$

To meet our goals, the matrix $\mathbf{D}$ and the vector $\mathbf{c}$ are chosen such that

$$\{\mathbf{D}\hat{\mathbf{v}} - \mathbf{c}\}_j = \frac{w_j}{P_j}\int_0^{P_j} dp\ [\upsilon_j^+(p) - \upsilon_j^-(p)]. \tag{24}$$

Here $\{\}_j$ is the jth component of the vector within the brackets, j is a station not at the end of a section (so that on either side there is a velocity profile), $\upsilon_j^+(p)$ and $\upsilon_j^-(p)$ are the total geostrophic velocity profiles at both sides of the station j, P_j is the depth of station j and finally w_j are weighting constants to be chosen later. Note that on the left-hand side of (24) we have the unknown barotropic velocity function, but on the right-hand side we have the total velocity field. With (24) as a minimization criterion, the jumps in the total geostrophic flow, caused by the piecewise-linear interpolation of the density are minimized. In this way the smoothest solution is determined, that extracts the maximum amount of information from the inverse equations.

When $\upsilon_j^+(p)$ and $\upsilon_j^-(p)$ are split into the barotropic and the baroclinic part, a more explicit expression for $\mathbf{W}$ and $\mathbf{c}$ can be given:

$$c_j = \frac{w_j}{P_j}\int_0^{P_j} dp\ [\tilde{\upsilon}_j^+(p) - \tilde{\upsilon}_j^-(p)], \tag{25}$$

and

$$\mathbf{D} = \begin{pmatrix} w_1 & -w_1 & 0 & 0 & \\ & w_2 & -w_2 & \ddots & \\ & & & w_j & -w_j \end{pmatrix}. \tag{26}$$

d. The dependence of the solution on the reference pressure p_0

An advantage of the minimization criterion given in (22) is that the resulting sum of the baroclinic and barotropic parts is independent of the a priori chosen reference level p_0. This will be demonstrated next. The baroclinic component was defined with respect to a level of no motion at $p = p_0$. When this level is changed, the

baroclinic component changes into $\tilde{\mathbf{v}}'(p) = \tilde{\mathbf{v}}(p) + \tilde{\mathbf{v}}^r$. Obviously, this change does not have an effect on $\mathbf{A}$ (and hence derived quantities like $\mathbf{V}_0$ and Λ) and $\mathbf{D}$. However, $\mathbf{b}$ is changed into $\mathbf{b}' = \mathbf{b} - \mathbf{A}\tilde{\mathbf{v}}^r$, and therefore the minimum norm solution changes into

$$\begin{aligned}\hat{\mathbf{v}}_0' &= \mathbf{V}\tilde{\mathbf{\Lambda}}\mathbf{U}^T\mathbf{b}' = \hat{\mathbf{v}}_0 - \mathbf{V}\tilde{\mathbf{\Lambda}}\mathbf{U}^T\mathbf{U}\mathbf{\Lambda}\mathbf{V}^T\tilde{\mathbf{v}}^r \\ &= \hat{\mathbf{v}}_0 - \tilde{\mathbf{v}}^r + \mathbf{V}_0\mathbf{V}_0^T\tilde{\mathbf{v}}^r, \end{aligned} \tag{27}$$

where use has been made of the identity $\mathbf{V}_0\mathbf{V}_0^T + \mathbf{V}\mathbf{J}_K\mathbf{V}^T = \mathbf{I}_M$. The effect of changing the reference level on the superposition of the barotropic and the baroclinic part is given by

$$\begin{aligned}\mathbf{v}'(p) &= \tilde{\mathbf{v}}'(p) + \hat{\mathbf{v}}_0' = \tilde{\mathbf{v}}(p) + \hat{\mathbf{v}}_0 + \mathbf{V}_0\mathbf{V}_0^T\tilde{\mathbf{v}}^r \\ &= \mathbf{v}(p) + \mathbf{V}_0\mathbf{V}_0^T\tilde{\mathbf{v}}^r. \end{aligned} \tag{28}$$

This is true for the total flow in the normal SVD approach, where the norm of the solution is minimized.

In our approach, however, (23) is used for the barotropic flow and the effect of changing the reference on $\mathbf{c}$ must be characterized. Since the difference in offset at the positive and negative side of station j is precisely given by the difference operator $\mathbf{D}$ applied on $\tilde{\mathbf{v}}^r$, we have

$$\mathbf{c}' = \mathbf{c} + \mathbf{D}\tilde{\mathbf{v}}^r. \tag{29}$$

The effect on the barotropic component is found by substituting (27) and (29) into (23),

$$\begin{aligned}\hat{\mathbf{v}}' &= \hat{\mathbf{v}}_0' - \mathbf{V}_0(\mathbf{V}_0^T\mathbf{D}^T\mathbf{D}\mathbf{V}_0)^{-1}\mathbf{V}_0^T\mathbf{D}^T(\mathbf{D}\hat{\mathbf{v}}_0' + \mathbf{c}') \\ &= \hat{\mathbf{v}}_0 - \tilde{\mathbf{v}}^r + \mathbf{V}_0\mathbf{V}_0^T\tilde{\mathbf{v}}^r - \mathbf{V}_0(\mathbf{V}_0^T\mathbf{D}^T\mathbf{D}\mathbf{V}_0)^{-1} \\ &\quad \times \mathbf{V}_0^T\mathbf{D}^T(\mathbf{D}\hat{\mathbf{v}}_0 - \mathbf{D}\tilde{\mathbf{v}}^r + \mathbf{D}\mathbf{V}_0\mathbf{V}_0^T\tilde{\mathbf{v}}^r + \mathbf{c}') \\ &= \hat{\mathbf{v}}_0 - \tilde{\mathbf{v}}^r + \mathbf{V}_0\mathbf{V}_0^T\tilde{\mathbf{v}}^r - \mathbf{V}_0(\mathbf{V}_0^T\mathbf{D}^T\mathbf{D}\mathbf{V}_0)^{-1} \\ &\quad \times \mathbf{V}_0^T\mathbf{D}^T(\mathbf{D}\hat{\mathbf{v}}_0 + \mathbf{D}\mathbf{V}_0\mathbf{V}_0^T\tilde{\mathbf{v}}^r + \mathbf{c}) \\ &= \hat{\mathbf{v}} - \tilde{\mathbf{v}}^r + \mathbf{V}_0\mathbf{V}_0^T\tilde{\mathbf{v}}^r - \mathbf{V}_0(\mathbf{V}_0^T\mathbf{D}^T\mathbf{D}\mathbf{V}_0)^{-1} \\ &\quad \times \mathbf{V}_0^T\mathbf{D}^T(\mathbf{D}\mathbf{V}_0\mathbf{V}_0^T\tilde{\mathbf{v}}^r) \\ &= \hat{\mathbf{v}} - \tilde{\mathbf{v}}^r, \end{aligned} \tag{30}$$

so that the total flow $\mathbf{v}'(p) = \tilde{\mathbf{v}}'(p) + \hat{\mathbf{v}}_0' = \tilde{\mathbf{v}}(p) + \hat{\mathbf{v}}_0 = \mathbf{v}(p)$ is independent of the reference level chosen.

Note that in Wunsch and Grant (1982) it has been derived that only the filtered version of the estimated velocity, in our symbols $(I_M - \mathbf{V}_0\mathbf{V}_0^T)\mathbf{v}$, is independent of the reference level.

e. Further smoothing of the solution

In practice it appears that many of the singular values of the matrix $\mathbf{A}$ are very close to zero. Mathematically this means that the inverse equations are almost linearly dependent and the solution of the inverse problem, Eq. (17), becomes unstable no matter what model for the null space is taken. The geometrical analogy is that two almost parallel lines intersect at infinity. A simple but ad hoc method to remove the instabilities is to set to zero all singular values smaller than some truncation value δ. In this way the norm of the solution is reduced to realistic values at cost of a small mismatch in the sum of the conserved transports. In this section the effects of truncation on the mismatch error will be quantified.

The truncation has an effect on the way $\tilde{\mathbf{\Lambda}}$ is derived from Λ. Instead of setting all zero singular values to infinite, all singular values smaller than δ are made infinite before taking the reverses. It will be assumed that the first K_δ singular values are larger than δ and the truncated $\tilde{\mathbf{\Lambda}}$ will be denoted by $\tilde{\mathbf{\Lambda}}_\delta$. To compute the mismatch error in case of truncation, it is convenient to express the vector $\mathbf{b}$ as

$$\mathbf{b} = \mathbf{U}\mathbf{m}. \tag{31}$$

Since $\mathbf{U}$ is an orthonormal, we have that $|\mathbf{b}| = |\mathbf{m}|$, so that $\mathbf{m}$ is a rotated version of $\mathbf{b}$. From (17) and (31) we find for $\varepsilon = \mathbf{A}\hat{\mathbf{v}} - \mathbf{b}$

$$\begin{aligned}\varepsilon &= \mathbf{U}\mathbf{\Lambda}\mathbf{V}^T\mathbf{V}\tilde{\mathbf{\Lambda}}_\delta\mathbf{U}^T\mathbf{U}\,\mathbf{m} + \mathbf{U}\mathbf{\Lambda}\mathbf{V}^T\mathbf{V}_0\mathbf{l} - \mathbf{U}\mathbf{m} \\ &= \mathbf{U}(\mathbf{J}_{K_\delta} - I)\mathbf{m} + \mathbf{U}\begin{pmatrix} 0 & & \mathbf{0} \\ \lambda_{K_{\delta+1}} & & \\ & \lambda_{K_{\delta+2}} & \\ \mathbf{0} & & 0 \end{pmatrix}\mathbf{l}. \end{aligned} \tag{32}$$

Here the matrix between $\mathbf{U}$ and $\mathbf{l}$ consists of the last $M - K_\delta$ columns of $\mathbf{\Lambda}$. For the minimum of $\varepsilon^T\varepsilon$, we find

$$\varepsilon^T\varepsilon = \sum_{k=K_{\delta+1}}^{K}(m_k + \lambda_k l_k)^2 + \sum_{k=K+1}^{M} m_k^2. \tag{33}$$

Here the m_k reflect the mismatch caused by the fact that $\mathbf{b}$ does not exactly lie in the range of (the truncated) $\mathbf{A}$. The physical meaning of this mismatch is that the measurements are not completely described by the model. The λ_k is an effect of the model used to describe the null space. This effect is, however, small because the λ_k in the sum of (33) were small by definition.

An alternative method to remove the effect of the small singular values is based on Bayes' estimation. If there is a priori information about the solution in statistical form, that is, if it is known that $\hat{\mathbf{v}}$ has a zero expectation value and a covariance matrix of $\sigma^2\mathbf{C}$, then the best possible estimate of $\hat{\mathbf{v}}$ based on the combination of experimental data and a priori knowledge is obtained by minimizing [see, e.g., Lorenc (1986) for a derivation]

$$\mathbf{H}_B = (\mathbf{A}\hat{\mathbf{v}} - \mathbf{b})^T(\mathbf{A}\hat{\mathbf{v}} - \mathbf{b}) + \sigma^2\hat{\mathbf{v}}^T\mathbf{C}\hat{\mathbf{v}}. \tag{34}$$

When nothing is known about the length scales involved, $\mathbf{C}$ is the identity matrix and the minimum of $\mathbf{H}_B$ is obtained by

$$\hat{\mathbf{v}} = \mathbf{V}\bar{\mathbf{\Lambda}}\mathbf{U}^T\mathbf{b}, \tag{35}$$

where $\bar{\mathbf{\Lambda}} = \mathrm{diag}[\lambda_i/(\lambda_i^2 + \sigma^2)]$. Clearly, σ^2 reduces the effect of λ_i^{-1} when λ_i is small. This way of smoothing is also known as ''tapering'' (Olbers 1989).

TABLE 2a. Results of simulation, conditions see Table 2b. Rms² is defined as $(I + II - III)^2 + (III + IV - V)^2 + (V - VI)^2$. The column cor is the number of sections that have the same sign as experiment C3. See text for the precise definition.

	Total transport						Transport section III					
	I	II	III	IV	V	VI	11	12	13	14	Rms²	cor
A1	.3	−2.2	−1.9	2.3	−0.5	0.3	1.9	0.0	−3.1	−0.6	1.44	−2
A2	.3	−2.1	−1.8	2.2	−0.5		1.8	0.0	−3.1	−0.6	0.71	−2
A3	.3	−2.1	−1.9				1.8	0.0	−3.1	−0.6	0.00	−2
A4			−5.4	6.7	1.2		0.9	−0.6	−4.9	−0.9	0.00	0
B1	.1	8.5	8.7	−4.9	3.2	3.2	5.8	2.5	−0.7	0.4	0.40	4
B2	−.6	0.0	−0.9	4.3	1.9	2.1	2.1	.2	−2.7	−0.6	2.30	1
B3	−.3	1.6	0.5	1.8	1.1	1.6	2.8	.6	−2.3	−0.6	2.40	3
C1	−.5	15.1	14.5	−10.6	3.6	3.6	7.4	3.5	3.6	0.0	0.16	4
C2	−.5	3.2	2.3	2.7	3.8	4.0	3.4	1.0	−1.5	−0.5	1.43	4
C3	−.2	5.0	4.0	0.1	3.0	3.5	4.0	1.3	−0.9	−0.5	2.02	4
D1	.3	6.6	7.1	−4.0	2.4	2.3	5.5	2.2	−0.1	−0.5	0.63	4
D2	−.8	0.0	−1.0	4.2	1.7	1.9	2.1	0.2	−2.7	−0.6	2.22	1
D3	−.5	1.3	0.1	2.0	0.8	1.3	2.7	0.5	−2.5	−0.6	2.29	3
E1	.2	7.2	7.5	−2.2	4.7	4.8	5.4	0.1	0.4	−0.4	0.37	4
E2	−.2	2.1	1.8	1.4	2.2	2.7	3.3	0.9	−1.8	−0.5	1.33	4
E3	−.4	2.6	1.7	.8	1.6	2.3	3.4	0.8	−1.7	−0.5	1.53	4
G1	−.8	−1.5	−2.5	2.7	−1.0		1.7	0.1	−3.4	−0.6	1.63	−3
G2	.2	7.5	8.2				6.0	2.5	−0.2	−0.4	0.27	2
G3			−2.1	2.3	−0.7		1.7	0.1	−3.2	−0.6	0.82	−2
H1	−.3	9.3	9.8	−6.9	2.2	2.3	6.2	2.7	1.2	0.3	0.51	4
H2	.6	3.6	2.7	0.2	1.7	1.9	3.3	0.9	−1.0	−0.4	1.71	4
H3	−.4	4.7	3.6	−2.4	0.3	0.7	3.7	1.2	−0.9	−0.4	1.50	3
I1	−2.4	15.2	12.8	−14.9	−3.0	−3.0	7.1	3.0	2.7	0.0	0.96	0
I2	−.6	3.4	2.8	4.0	5.9	6.0	4.3	1.0	−1.9	−0.6	0.87	4
I3	.6	6.3	5.9	1.3	6.3	6.7	5.5	1.6	−0.8	−0.5	1.12	4
J1	−.4	−3.2	−4.3	3.1	−2.2		1.0	−0.4	−4.1	−0.8	1.48	−3
J2	−2.0	10.6	8.9				6.7	2.1	0.4	−0.3	0.14	2
J3			−3.5	−1.0	−5.7		0.9	−0.4	−3.4	−0.6	0.48	−2
	E	N	E	N	E	E			E		Sv	

4. Results and comparison

In this section several variants of the inverse model given in section 3 are applied on the 1991 data and compared. For each variant, the transports through each section of Fig. 2 and each layer of Fig. 4 were computed. To save space, only the total transports through each section are presented (Tables 2a and 2b) and only the transport through section III is divided into different layers. In all computations, the wind-driven layer was removed by disregarding all water masses above 100 m. Since all three boxes are almost completely bounded by sea, the net mass flow into this top layer will add up to about zero, automatically. Therefore, its omission will have a small effect on the results, which was verified in separate experiments (not presented here). All transports are expressed in Sverdrups.

The symbol in the first column of Table 2a refers to the precise computation method (summarized in Table 2b). Columns 2–7 give the total transport through section I to VI, columns 8–11 give the transports through layers 1–4 of section III, and column 12 gives the sum of squared errors of the net transports through the boxes involved in the computations. Note that in the inverse methods this is not the optimized quantity. The optimized quantity is the sum of squared errors over all boxes and all layers, and therefore this quantity is not comparable for all experiments.

To compare the distributions of the total transports through all sections, the following correlation coefficient was used (last column of Table 2a):

$$\mathrm{cor}(\mathrm{X}, \mathrm{Y}) = \sum_{i=1}^{6} \mathrm{sgn}(x_i)\ \mathrm{sgn}(y_i), \tag{36}$$

with

$$x_i \equiv \begin{cases} \text{transport } i \\ 0 \end{cases} \quad \text{if} \quad \begin{cases} |\text{transport } i| > 0.5 \text{ Sv} \\ |\text{transport } i| \le 0.5 \text{ Sv}. \end{cases} \tag{37}$$

Here, X and Y refer to different experiments. The effect of taking the sign of the transport, instead of the transport itself, is that the correlation coefficient is not dominated by large transports that appear if small singular values are included. The threshold of 0.5 Sv prevents the correlation coefficient from being dominated by small transports (with almost arbitrary signs). The correlation coefficient defined by (36) ranges between −6 and +6. Coefficients of 3 or larger are considered as ''large.''

In the first computation method an optimal level of no motion was used, as described in section 2. In experiment A1 all boxes were used, in experiment A2 the right most box was removed, in experiment A3 the middle and the right boxes were removed, and in experiment A4 only the middle box was used. The purpose of these

TABLE 2b. Abbreviations are l.n.m.: optimal level of no motion, SVD: minimum normal solution (no weighting), DIF: maximum smoothing (no weighting), W: minimum weighted norm, WDIF: minimum weighted differences, pref: reference level, trunc: truncated inverse model matrix, tap: tapered least squares, and lmr: left middle or right boxes.

	Null-space	Pref	Smoothing	Level	Layers	Boxes
A1	l.n.m.	1009				lmr
A2	l.n.m.	1015				lm
A3	l.n.m.	1013				l
A4	l.n.m.	717				m
B1	SVD	1000	trunc	0.1%	4	lmr
B2	SVD	1000	trunc	1.0%	4	lmr
B3	SVD	1000	trunc	1.0%	8	lmr
C1	DIF		trunc	0.1%	4	lmr
C2	DIF		trunc	1.0%	4	lmr
C3	DIF		trunc	1.0%	8	lmr
D1	W	1000	trunc	0.1%	4	lmr
D2	W	1000	trunc	1.0%	4	lmr
D3	W	1000	trunc	1.0%	8	lmr
E1	W	1000	tap	0.1%	4	lmr
E2	W	1000	tap	1.0%	4	lmr
E3	W	1000	tap	1.0%	8	lmr
G1	W	1000	trunc	1.0%	4	lm
G2	W	1000	trunc	1.0%	4	l
G3	W	1000	trunc	1.0%	4	m
H1	W	1300	trunc	0.1%	4	lmr
H2	W	1300	trunc	1.0%	4	lmr
H3	W	1300	trunc	1.0%	8	lmr
I1	WDIF		trunc	0.1%	4	lmr
I2	WDIF		trunc	1.0%	4	lmr
I3	WDIF		trunc	1.0%	8	lmr
J1	WDIF		trunc	1.0%	4	lm
J2	WDIF		trunc	1.0%	4	l
J3	WDIF		trunc	1.0%	4	m

experiments was to find out how sensitive the method is to the unwanted omission of planned measurements. It was found that the optimal levels of no motion were 1009, 1015, 1013, and 717 dbar respectively. Since these levels are very close (except A4), it is not surprising that the transports shown in Table 2 are also very similar. Consequently, the transport through section II is highly independent of the measurements on section V when the optimal level of no motion is used. The reason why the result for experiment A4 is rather different is that, contrary to A1–A3, the minimum was very flat. For instance, the rms error at 1000 dBar was only 0.2 Sv. Note that in experiments A3 and A4 there was only one box and the sum of squared errors consists of only one term. Therefore, the rms error can be made zero exactly in these cases.

In experiments B1–B3 the minimum norm solution was computed according to (21). Slightly different conditions were used in B1, B2, and B3. In experiments B1 and B2, the conservation laws were applied to the four layers depicted in Fig. 4. In B1 the truncation level of the singular value decomposition was set at 0.1% and in B2 at 1 %. In B3 the truncation was also set to 1 %, but the water column was divided into eight layers defined by equal differences in potential density (as shown in Fig. 7). Table 2 shows that the results for B2 and B3 are rather similar [cor(B2, B3) = 3]. In experiment B1, however, there is a rather strong northward transport through section II and a strong eastward transport through section III. These transports are absent in the other experiments [cor(B1, B2) = 0]. The lower residual and the larger transports in B1 are in accordance with the theory presented in section 3. In other experiments, not shown here, it appeared that the minimum norm solution is quite sensitive to the omission of boxes and the division into layers when a small truncation value is applied.

When instead of the norm, the vertically integrated differences of subsequent stations were minimized, Eqs. (25) and (24), the results labeled with C1, C2, and C3 were obtained. The truncation levels and division into layers corresponds to B1, B2, and B3. Similar to the minimum norm solution, the division into layers has only a minor effect on the result (cor(C2, C3) = 4). There also is a large similarity between B1 and C1, B2 and C2, and between B3 and C3, which is illustrated by the respective correlations: 5, 2, and 3.

In Fig. 8, the complete current pattern of experiment C3 is depicted. Note that there is a negative correlation with A2 (Fig. 3). However, both figures show a strong northeastern current in the upper layer. In the case of the optimal level of no motion, this current is compensated by a return current at the level of the LSW. This return current is absent in the results of C3, and therefore the directions of the total mass transports are completely reversed.

If instead of the simple minimum norm a weighted minimum norm is used [Eq. (22) with $\mathbf{c} = \mathbf{0}$ and $\mathbf{W} = \text{diag}(\text{area}_m)$] as proposed by Wunsch, then the results D1, D2, and D3 are obtained. Again, the number of layers only has a small effect (cor(D2, D3) = 3). When the smoothing was realized by tapering, as was done in experiments E1–E3, the results were similar: cor(E1, D1) = 5, cor(E2, D2) = 2, and cor(E3, D3) = 4.

In experiments G1–G3 the sensitivity of the weighted minimum norm to the omission of measurements is demonstrated. Here, different combinations of boxes were used, all with the same truncation level (1 %) as in D2 and the same layers as in D2. If only the right box is omitted (G1), the resulting transports show some similarity to D2 (cor(G1, D2) = 2). However, if both the right and the middle boxes are left out of the computations, the correlation with D2 is very low: cor(D2, G2) = −1. If only the middle box is included, as in experiment G3, the correlation with D2 equals 1. The large sensitivity of the current pattern to the omission of boxes is further shown in the last column of Table 2A: the correlations with C3 are −3, 2, and −2, respectively.

The weighted minimum norm is dependent on the initial reference level. This is demonstrated in experiments H1–H3, for two truncation levels and two layer distributions, where all conditions were similar to ex-

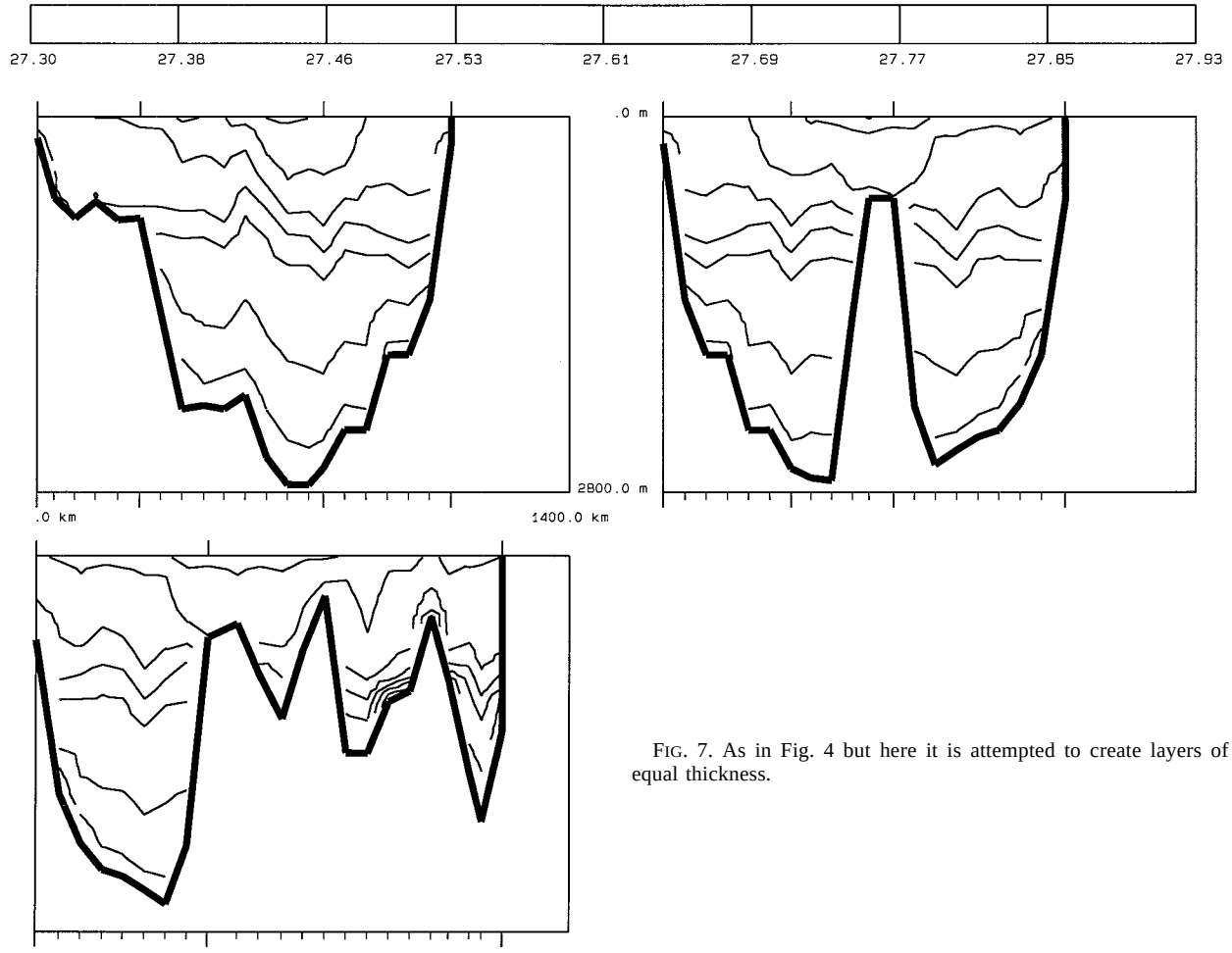

FIG. 7. As in Fig. 4 but here it is attempted to create layers of equal thickness.

periments D1–D3, except the reference level, which was set equal to 1300 dbar. This reference level is closer to the level of minimum variability than the 1000-dbar level. A comparison of transports by means of the correlation coefficients shows cor(D1, H1) = 5, cor(D2, H2) = 0, and cor(D3, H3) = 1. This demonstrates that the effect of the reference level is substantial.

In experiments I1–I3 and J1–J3 it was attempted to combine the weighting method of Wunsch with the criterion of minimized vertically integrated differences. This was achieved by using (22), (25), and (26) with $w_j = P_j$. It appears that this way of weighting has a strong effect when a small truncation level is used: cor(C1, I1) = 1, cor(C2, I2) = 5, and cor(C3, I3) = 4. The number of boxes included in the method has a dramatic effect on the results (as in G): cor(I2, J1) = −2, cor(I2, J2) = 3, and cor(I2, J3) = −3. This effect is further demonstrated in the last column of Table A2, where a comparison with C3 is made.

When it is assumed that the previous experiments are representative of the infinitely many experiments that could be done, the following general conclusions may be drawn:

1) The mean transport over section I (the Reykjanus Ridge) is probably smaller than 1 Sv, but its direction cannot be determined.
2) The mean transport over section IV is directed to the east; its amplitude ranges between 1 and 4 Sv.
3) When a truncation value of 0.1 % is used, this results in large (compensating) transports. The direction of these transports is very systematic: north on section II, east on section III, and south on section IV. A problem is that for a larger truncation value, these transports can have any direction.
4) The comparison on the basis of the correlation coefficient shows that the removal of complete boxes has the dramatic effect on the estimation of the directions of the transports.

The latter two conclusions indicate that the inverse method hardly improves the solution obtained with a level of no motion. The results were diverging even further when more layers were included, other boxes were left out, other tracers were used, and when all these conditions were combined in different ways.

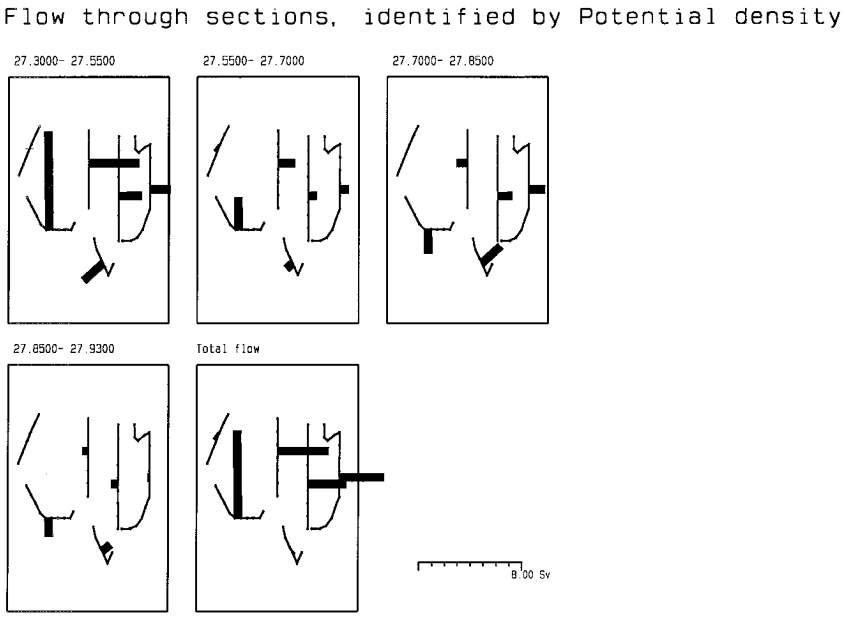

FIG. 8. Transports for the 1991 dataset, using the maximum smoothness criterium. The precise parameters of the applied inverse model correspond to case C3 of Table 2.

5. A simulation with an alternative sampling strategy

One might argue that the weighted minimum norm solution is based on a more or less ad hoc argument. The other solutions presented in Table 2 all have a rather small rms error, and they are all based on sensible models for the null space and therefore they represent equally valid candidates for the pattern of transports in the Iceland basin. To find out whether the large variations in the solutions are caused by the noise of high spatial frequency present in our dataset, a similar series of computations was performed using the Levitus climatological dataset (Levitus 1982) of the same area. The sampling scheme used for these computations is shown in Fig. 9. The computations resulted in a table comparable to that of Table 2: there were large sensitivities for the number of boxes, truncation levels, etc., even though the Levitus dataset is highly smoothed.

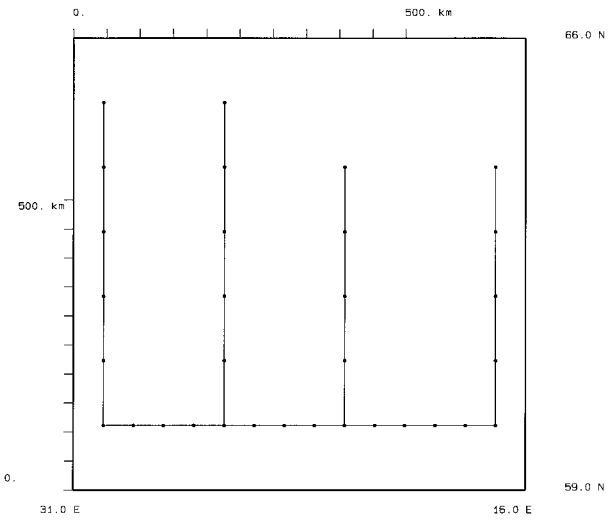

FIG. 9. Levitus sampling scheme corresponding to Fig. 2.

The central difficulty in the estimation procedure is that the inverse equations are not restrictive enough to determine a unique solution. There are six sections through which the transports are to be computed and a simple mass balance gives only three equations. When the mass balance is applied to the individual layers, this results in equations that are very much dependent on the three equations for the complete boxes. This is demonstrated in Fig. 10, where the distribution of the singular values is logarithmically plotted for some of the experiments described in Table 2.

In Fig. 10a the singular values correspond to experiment G2. There is only one box that is divided into four layers, which yields four equations and four nonzero singular values. The first singular value is dominating (~85%), the second one is less than 10%. In Fig. 10b the number of boxes is increased to 2 (experiment G1), and the boxes are divided into four layers each. The eight singular values are dominated by the first two, which are the only singular values larger than 10%. When the boxes are divided into more layers, the additional equations do not increase the amount of information because only small singular values are added. This is demonstrated in Fig. 10c, where three boxes were used and the conserved tracers were potential density, oxygen, and phosphate. It appears that only three singular values are larger than 10%. The general conclusion

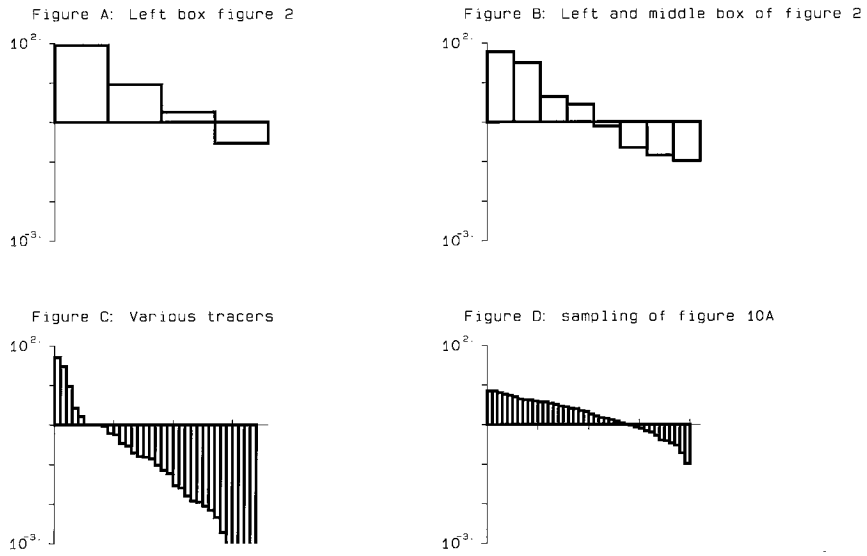

FIG. 10. Distribution of the (squares) of singular values plotted on a logarithmic scale for different sets of computations. (a) Experiment G2 of Table 2 and (b) G1. (c) Various tracers were used. (d) The sampling scheme presented in Fig. 11a.

from these plots is that the number of ''truly'' independent equations is highly related to the number of boxes.

It is expected that a much more favorable distribution of the data points is obtained when the number of boxes is large compared to the number of sections. Such sampling schemes are given in Fig. 11. The interstation distance is one degree (which corresponds to 60 km in the *x* direction and 110 km in the *y* direction), and the station positions coincide with the Levitus dataset. In order to find out if this sampling scheme indeed gives more stable results, some simulations were performed.

For each triangular box it is assumed that only the total mass is conserved. In the case of Fig. 11a this gives 40 equations and 79 unknown flows. The distribution of the singular values of the matrix **A**, ordered from large to small, is shown in Fig. 10d. This shows that the singular values are much more evenly distributed than in the cases presented in the previous section. Therefore, it may be expected that if the transports through five surrounding sections are computed, the results will be more stable than in the conventional configuration. Although no truncation was applied, the maximum transport that occurred was only 2.2 Sv, so that the ''blow up effect'' present in the cases of previous sections is diminished. Therefore, in this case there is no need to introduce a truncation parameter and study its effect. If, however, the singular values smaller than 0.1% are made zero, the computed transports were hardly different. Furthermore, the results shown in Table 3 have a clear interpretation: there is a superficial layer flowing to the northeast and a return current at the bottom flowing in the opposite direction.

In the conventional configuration, leaving out one box had a major effect on the unweighted solution. When in the alternative sampling scheme the right-hand side was left out (Fig. 11b) or when both the left- and right-hand sides were left out (Fig. 11C), very similar qualitative and quantitative transports were obtained, see Table 3. In this way the stability of the alternative sampling scheme has been demonstrated, at least for an idealized dataset.

6. Discussion

The main issue raised in the present paper is whether it is possible to extract physically meaningful information from a linearly dependent and underdetermined set of inverse modeling equations. This question is closely connected to the discussion between Wunsch (1985, 1986) and Veronis (1986) in ''recent'' oceanographic literature. This discussion was triggered by a simulation study of Fiadeiro and Veronis (1984) on the possibility of estimating the two-dimensional flow pattern based on tracer measurements. They concluded that this was impossible, unless enough data were sampled to obtain an overdetermined system. The main argument of Wunsch against this conclusion was that by using special mathematical estimation techniques it remains possible to estimate at least the large-scale flow pattern.

The inverse problem treated here is different from the studies of Fiadeiro and Veronis (1984) and, since we did not have information about the true velocity field, we could only study the stability of the solution, not its reliability. On the basis of our results it may be concluded, similar to Fiadeiro and Veronis, that there are substantial intrinsic limitations to a successful application of inverse modeling of hydrographic data. On the other hand, the simulation studies with the alternative sampling scheme yielded physically relevant results, but

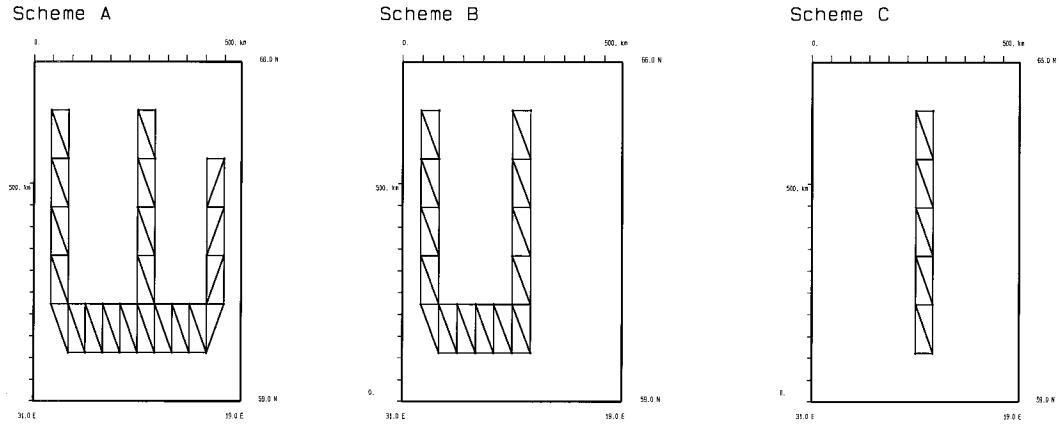

FIG. 11. An alternative way of sampling the same area as Fig. 2. By following a zig-zag course, many more boxes can be created upon which the conservation principles can be applied. (a) All zig-zag sections included, (b) right-hand part removed, (c) left- and right-hand side removed.

the underlying system of equations is still formally underdetermined. This result seems to support the standpoint of Wunsch. The central question is: How should one count the number of unknowns and the number of equations? If only the mass balance is taken into account for each box and if one assumes that the other equations are linearly dependent from it, then the number of equations equals the number of boxes. If for the number of unknowns one counts the number of station pairs, the mathematical system is underdetermined in either sampling scheme. But if, on the other hand, the number of sections is counted, we have an overdetermined system in the alternative sampling scheme and an underdetermined system in the conventional sampling scheme.

The unfavorable distribution of singular values reported in the present study is well comparable with the findings of Fiadeiro and Veronis (1982). In their study, an inverse model was derived for one box consisting of four layers. From the numbers given in their paper it can be computed that the distribution of singular values is 94.22%, 4.73%, 1.01%, and 0.04%. This distribution shows that there is essentially one equation per box and therefore large instabilities can be expected if the inverse model would be applied to compute transports through sections bounding the box.

The alternative sampling scheme studied here has some similarity with the ones used by others. For instance, in Tziperman (1988) a hydrographic dataset consisting of a 2D grid was used to study the oceanic circulation and mixing coefficients. This sampling scheme made it possible to include unknown mixing coefficients without creating an underdetermined system. In Lee and Veronis (1991, 1993) a 2D data grid was used to compare the velocity patterns determined by geostrophy and by tracer advection. Also, in large-scale studies of the entire North Atlantic, by, for example, Olbers et al. (1985), Hogg (1987), and Bogden et al. (1993), 2D grids (of Levitus data) were analyzed with inverse modeling techniques.

TABLE 3. The effect of leaving out one or two branches of the sampling scheme (Fig. 11), upon the distribution of transports through the middle section of Fig. 11A. Transports are in Sverdrups: positive flow is directed toward the east.

Layer	A	B	C
27.20–27.52	.68	.64	.65
27.52–27.62	−.27	−.30	−.30
27.62–27.75	−.36	−.39	−.38
27.75–27.83	−.41	−.43	−.42 Sv

The purpose of the present paper, however, was to explore the possibilities of extracting the mass transports from a regional synoptic dataset. A full 2D sampling scheme of a large oceanic area is far beyond the practical possibilities. The sampling scheme studied in the present paper may be considered as a compromise between a full 2D scheme (with high stability) and the 1D section scheme (which covers a large area but may become unstable). The proposed scheme could be applied in practice by following a zigzag course and could therefore be realized in about twice the time needed for the conventional sampling scheme. Moreover, the sampling scheme presented in this paper could be further optimized using, for example, the approach of Barth and Wunsch (1990).

Compared to the ''normal'' way of sampling, the alternative sampling scheme has the advantage that the data corresponding to the same box is more synoptic. It takes perhaps only half a day to perform three stations, the corners of the proposed boxes, and therefore it is much more likely that the data can be treated as synoptical than in the ''normal'' case, where it may take more than a week to close a box. Other theoretical advantages are that

1) the stability is obtained without assuming more than conservation of mass so that no division into layers

is necessary. This appeared to be a critical assumption of the inverse model.
2) the required scaling of the the ocean becomes more favorable for assuming stationarity (6).
3) there is no need to truncate the SVD solution, which eliminates an important source of subjectivity.

However, the author is well aware that the practical usefulness for real data still has to be demonstrated.

Acknowledgments. A travel grant of the Netherlands Organization for Scientific Research (NWO) is gratefully acknowledged. The author thanks Prof. Dr. J. T. F. Zimmerman, Dr. H. M. van Aken, Dr. L. Maas, and Dr. P. J. van Leeuwen for their valuable comments and suggestions.

APPENDIX

Data Interpolation

The interpolation of the data can be performed in many different ways. The basic idea behind most interpolation methods is to express the data as a linear combination of a set of base functions, which are functions of the horizontal coordinate s and the vertical coordinate p, and to determine the coefficients of this expansion by requiring that the differences between the interpolated and measured values is minimal. The choice of the base functions is relatively arbitrary. In this study we choose base functions derived from a triangulation of the data points. With a triangulation of the data points it is meant that the surface S, on which the measurement points are located, is divided into a set of nonoverlapping triangles of which the union equals S, and of which the corner points coincide with measurement points. On each triangle the interpolated value is a linear combination of the values at the corners of the triangle. If the triangle is given by the points (s_1, p_1), (s_2, p_2), and (s_3, p_3) at which the measured quantities take on the values f_1, f_2, and f_3, then the interpolated value at (s, p) equals

$$\begin{aligned} f(s,p) = {} & f_1[(s-s_2)(p_2-p_3)+(s_3-s_2)(p-p_2)]/d \\ & + f_2[(s-s_3)(p_3-p_1)+(s_1-s_3)(p-p_3)]/d \\ & + f_3[(s-s_1)(p_1-p_2)+(s_2-s_1)(p-p_1)]/d, \end{aligned} \tag{A1}$$

with

$$d \equiv (s_3 - s_1)(p_1 - p_2) + (s_2 - s_1)(p_3 - p_1), \tag{A2}$$

which appears to be twice the area of the triangle. It is readily verified that a substitution of (s_k, p_k) into (A1) yields f_k, for $k = 1, 2, 3$.

Interpolation with a triangulation and functions like (A1) yield piecewise linear fields, which are continuous at the edges of the triangles. The advantages of interpolation with these base functions are:

1) The interpolated fields depend only on the surrounding measurements and are not disturbed by the propagation of errors in far away measurements.
2) This interpolation method does not create artificial minima or maxima. Instead, the minima and maxima are located at the corners of the triangles, that is, at the measurement points themselves.
3) The base functions have a relatively simple mathematical form, which facilitates mathematical operations like integrations and differentiations.

A minor disadvantage is that the method requires a rather inconvenient way of ''bookkeeping'' of indices. This bookkeeping is further complicated by the use of neighboring boxes with common boundaries.

The measurement points have the coordinates (s_j, p_{ji}), $j = 1, \cdots, J$ and $i = 1, \cdots, I_j$. Here the index i refers to the ith measurement at station j. The depths and the number of depths I_j may vary from station to station and they may also vary from tracer to tracer. The basic idea behind the triangulation scheme proposed here is that for each pair of stations m, a set of triangles is defined which consists of two ''horizontal'' edges (connecting measurement points of two subsequent stations on a section) and one vertical edge (which connects two measurements at the same station). The result of this triangulation is shown in Fig. 6.

To apply the above triangulation on the computation of the baroclinic velocity, we first compute at each point (s_j, p_{ji}) the inverse of the density, $1/\rho_{ji}$. Then the $1/\rho$ field is interpolated using (A1) and differentiated in the s direction. We obtain

$$\frac{\partial}{\partial s}\frac{1}{\rho} = \frac{p_{k2} - p_{k3}}{d\rho_{k1}} + \frac{p_{k3} - p_{k1}}{d\rho_{k2}} + \frac{p_{k1} - p_{k2}}{d\rho_{k3}}, \tag{A3}$$

where in this case d simplifies to

$$d = (s_{j2} - s_{j1})(p_{k3} - p_{k1}), \tag{A4}$$

where $j1$ and $j2$ are used to denote the two stations and k_1, k_2, and k_3 refer to the bottle numbers at the corners of the triangle.

Since (A3) is independent of s and p, a piecewise constant function is obtained, that is, a function that is constant on each triangle, but which may jump if (s, p) is moved over the edge of a triangle. If (A3) is integrated over p, then the baroclinic velocity field $\tilde{v}(s, p)$ so obtained is again a piecewise linear function, at least in the direction of the p coordinate. However, if p is kept fixed and s is varied, then $\tilde{v}(s, p)$ will vary linearly until s goes from one station pair to the next, where $\tilde{v}$ will jump.

The advantage of computing the baroclinic velocity in this way is that it automatically gives an estimate of the baroclinic velocity at the bottom end of two stations of unequal depth, without making special assumptions. The jumps that occur in $\tilde{v}(s, p)$ are not a particular disadvantage of the triangulation method; they also occur when $\tilde{v}(s, p)$ is computed in the conventional way.

REFERENCES

Apel, J. R., 1987: *Principles of Ocean Physics.* Int. Geophys. Ser., Vol. 38, Academic Press, 102 pp.

Barth, N., and C. Wunsch, 1990: Oceanographic experiment design by simulated annealing. *J. Phys. Oceanogr.,* **20,** 1249–1263.

Berthero, M., C. de Mol, and E. R. Pike, 1988: Linear inverse problems with discrete data: II stability and regularization. *Inv. Prob.,* **4,** 573–594.

Bogden, P. S., R. E. Davis, and R. Salmon, 1993: The North Atlantic circulation: Combining simplified dynamics with hydrographic data. *J. Mar. Res.,* **51,** 1–52.

Fiadeiro, M. E., and G. Veronis, 1982: On the determination of absolute velocities in the ocean. *J. Mar. Res.,* **40**(Suppl.), 159–182.

——, and ——, 1984: Obtaining velocities from tracer distributions. *J. Phys. Oceanogr.,* **14,** 1734–1746.

Fu, L. L., 1981: The general circulation and meridional heat transport of the subtropical South Atlantic determined by inverse methods. *J. Phys. Oceanogr.,* **11,** 1171–1193.

Harvey, J. G., and A. Theodory, 1986: The circulation of Norwegian Sea overflow water in the eastern North Atlantic. *Oceanol. Acta,* **9**(4), 393–402.

Hogg, N. G., 1987: A least-squares fit of the advective-diffusive equations to the Levitus Atlas data. *J. Mar. Res.,* **45,** 347–375.

LeBlond, P. H., and L. A. Mysac, 1978: *Waves in the Ocean.* Elsevier Oceanogr. Ser., Vol. 20, Elsevier, 459 pp.

Lee, J. H., 1993: A review of tracer inverse problems in oceanography. *Ocean Res.,* **15**(1), 53–69.

——, and G. Veronis, 1991: On the difference between tracer and geostrophic velocities obtained from C-SALT data. *Deep-Sea Res.,* **38**(5), 555–568.

——, and ——, 1993: Inversions of data from the thermohaline staircase in the western tropical North Atlantic. *Deep-Sea Res.,* **40**(9), 1839–1862.

Levitus, S., 1982: *Climatological Atlas of the World Ocean.* NOAA Prof. Paper No. 13, U.S. Govt. Printing Office, 173 pp.

Lorenc, A. C., 1986: Analysis methods for numerical weather prediction. *Quart. J. Roy. Meteor. Soc.,* **112,** 1117–1194.

McCartney, M. S., 1992: Recirculating components to the deep boundary current of the northern North Atlantic. *Progress in Oceanography* Vol. 29, Pergamon, 283–383.

McIntosh, P. C., 1990: Oceanographic data interpretation: Objective analysis and splines. *J. Geophys. Res.,* **95**(C8): 13 529–13 541.

Olbers, D., 1989: A geometrical interpretation of inverse problems. *Oceanic Circulation Models: Combining Data and Dynamics,* D. L. T. Anderson and J. Willebrand, Eds., Kluwer, 79–93.

——, and J. Willebrand, 1984: The level of no motion in an ideal fluid. *J. Phys. Oceanogr.,* **14,** 203–212.

——, M. Wenzel, and J. Willebrand, 1985: The inference of the North Atlantic circulation patterns from climatological hydrographic data. *Rev. Geophys.,* **23**(4), 313–356.

Roemmich, D., 1980: Estimation of meridional heat flux in the North Atlantic by inverse methods. *J. Phys. Oceanogr.,* **10,** 1972–1983.

——, 1981: Circulation of the Caribbean Sea: A well resolved inverse problem. *J. Geophys. Res.,* **86**(C9), 7993–8005.

Stommel, H., and G. Veronis, 1981: Variational inverse method for study of ocean circulation. *Deep-Sea Res.,* **28A**(10), 1147–1160.

Tziperman, E., 1988: Calculating the time-mean oceanic circulation and mixing coefficients from hydrographic data. *J. Phys. Oceanogr.,* **18,** 519–525.

——, and A. Hecht, 1988: Circulation in the eastern Levantine basin determined by inverse methods. *J. Phys. Oceanogr.,* **18,** 506–518.

Van Aken, H. M., 1988: Transports of water masses through the Faroese Channels determined by an inverse method. *Deep-Sea Res.,* **35**(4), 595–617.

——, 1997: Mean currents and current variability in the Iceland Basin. *J. Phys. Oceanogr.,* in press.

Veronis, G., 1986: Comments on ''Can a tracer field be inverted for velocity?'' *J. Phys. Oceanogr.,* **16,** 1727–1730.

——, 1987: Inverse methods for ocean circulation. *General Circulation of the Ocean,* H. D. I Abarbanel and W. R. Young, Eds., Springer, 102–133.

Wunsch, C., 1978: The North Atlantic general circulation west of 50°W determined by an inverse method. *Rev. Geophys. Space Phys.,* **16**(4), 583–620.

——, 1985: Can a tracer field be inverted for velocity? *J. Phys. Oceanogr.,* **15,** 1521–1531.

——, 1986: Reply. *J. Phys. Oceanogr.,* **16,** 1731–1732.

——, and B. Grant, 1982: Towards the general circulation of the North Atlantic Ocean. *Progress in Oceanography,* Vol. 11, Pergamon, 1–59.